Mass asymmetry dependence of elliptical flow at intermediate energy

Dissertation submitted for the partial fulfilment of requirement for
The award of the degree of

Master of Science

In

Physics

Submitted by
Sangeeta
Roll no. 301104013
Under the guidance of
Dr. Suneel Kumar

School of physics and Material Science
Thapar University
Patiala – 147004 (PUNJAB)
INDIA

CERTIFICATE

I hereby declare that the report entitled "**Mass asymmetry dependence of elliptical flow at intermediate energy**" is an authentic record of my own work carried out for the partial fulfilment of the requirement for the award of the degree of M.Sc. (Masters of Science) at Thapar University, Patiala (Punjab), under the guidance of Dr. Suneel Kumar (School of Physics and Materials Science). The matter presented in the dissertation has not been submitted in part or full for the award of any other degree.

Date: 13-June-2013

Sangeeta

Sangeeta

Roll No. : 301104013

It is certified that the above statement made by the candidate is correct to the best of my knowledge and belief.

SKumar

(Dr. Suneel Kumar)

Associate Professor

School of Physics and Materials Science

Thapar University, Patiala

(Dr. Kulvir Singh)

(Head)

School of Physics and Materials Science

Thapar University, Patiala

(Dr. S.K. Mohpatra)

Dean of Academic Affairs

Thapar University, Patiala

ACKNOWLEDGEMENTS

Foremost, I would like to express my sincere gratitude to my supervisor **Dr. Suneel Kumar** for his continuous support and supervision, for his patience, motivation, enthusiasm, and immense knowledge. His guidance helped me at all times of research and in writing this dissertation. I could not have imagined having a better advisor and mentor for my thesis.

I would like to thank **Dr. Kulvir Singh**, Head, School of Physics and Materials Science for his support and providing me the necessary lab facilities.

I express my deepest gratitude to **Mr. Karan Singh Vinayak and Miss Anupriya Jain**, without whom I would not have been able to complete my dissertation. My sincere thanks to the research scholars of the physics department for their help and valuable suggestions.

Special thanks to my friends **Amandeep Kaur, Reema, Sahil, Ajitpal Singh, Mandeep Kaur** and **Navjot Kaur** who helped me at every step during this work and staffs at the School of Physics and Material Sciences for providing me a friendly atmosphere and encouraging me throughout this work.

I am deeply thankful to my family, for their moral support and patience which gave me the necessary motivation and strength to endure research and complete my thesis. A special word of thanks to my brother and best friend **Naresh** for his encouragement towards my studies.

Above all I render my gratitude to Almighty who bestowed me the strength and vision to walk on the path of truth.

Date: 13-June-2013

Sangeeta

Sangeeta

Place: Thapar University, Patiala

Roll No. 301104013

Contents

Chapter 1 Introduction

Chapter 2 Methodology

Chapter 3 Elliptical flow in mass asymmetric collisions

List of figures

Abstract

The present work deals with the theoretical study of the elliptical flow for mass asymmetric collisions by means of Isospin-dependent Quantum Molecular Dynamical (IQMD) model. The work focuses on the study of sensitivity of elliptical flow towards Coulomb potential and symmetry energy for mid-rapidity region at energy 50 MeV/nucleon by using soft equation of state. Our results show that Coulomb interaction potential dominates the reaction dynamics over symmetry energy. Elliptical flow is strongly affected by the mass asymmetry of the colliding nuclei.

Chapter 1

Introduction

1.1 Heavy Ion Collisions

Heavy ion collisions (HIC's) mainly concern the investigation of nuclear matter under the extreme conditions of density and temperature. Some of the properties of nuclear matter are nuclear size ($R = R_o A^{1/3}$, where R_o=1.12), nuclear density (10^{17}kg/m^3), binding energy, nuclear forces, shape of the nucleus (oblate, prolate, spherical), interaction among nucleons and nucleon-nucleon scattering [1]. Heavy ion (which has mass number greater than and equal to the mass of alpha particle) collision provide a possibility for studying the bulk properties of nuclear matter under the condition vastly different than in normal conditions such as high density, high temperature and excitation as well as large difference in the proton and neutron number [2]. Nuclear equation of state (NEOS: equation that describes the relation between energy, pressure, temperature and density of the heated nuclear matter) and liquid gas phase are known as bulk properties of nuclear matter that is helpful to understand phenomena's like origin of early universe, big bang, supernova explosions, neutron star etc. [3]. On the basis of incident energy, the heavy ion physics can be classified into three groups:

a) Low energy heavy ion physics **(E < 10 MeV/nucleon).**

b) Intermediate energy heavy ion physics **(10 MeV/nucleon ≤ E ≤ 2 GeV/nucleon).**

c) High energy heavy ion physics **(E > 2 GeV/nucleon).**

HIC's at low incident energy (E < 10 MeV/nucleon) are useful to look at the low density phenomena also called physics of sub-density phenomenon. At low incident energy the colliding nuclei do not compress each other therefore, 98% of collisions are

blocked due to lack of availability of free phase space. Thus, dynamics at low energies is governed by the mean field only [4-6].

At low incident energies the nucleon-nucleon collisions are negligible and mean field is maximum, therefore the low energy nuclear reactions give unique possibility to look for the nuclear interactions, structure of nuclei, fusion, fission, γ-spectroscopy, cluster radioactivity, formation of super heavy nuclei and the halo nuclei etc. Fig.1.1 shows the reaction dynamics of heavy ion collision at low incident energy. When a projectile nucleus hits the target nucleus with energy lying in the low energy domain, form an excited state of nucleus called compound nucleus which further decays through various channels as shown in Fig.1.1.

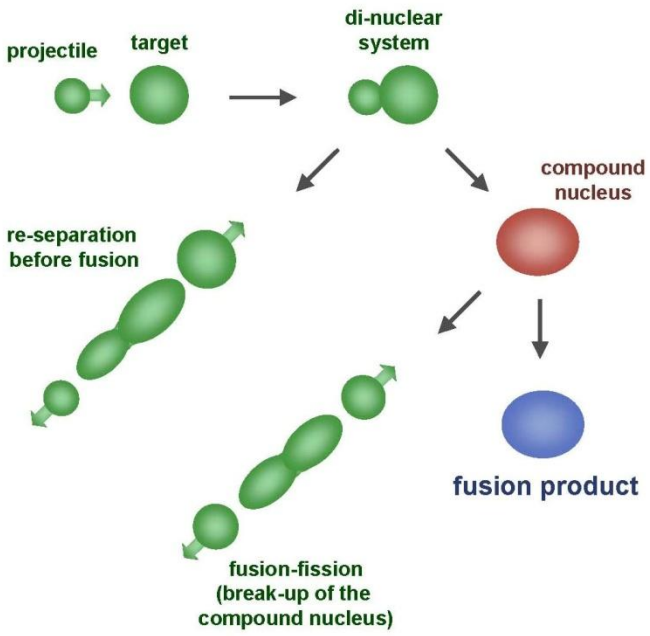

Fig.1.1: Reaction dynamics of HIC's at low incident energy.

In high energy heavy ion physics (E > 2 GeV/nucleon), the temperature and density are very high; one may have the quark gluon plasma. At very high energy there is availability of large phase space which makes the role of Pauli blocking is negligible.

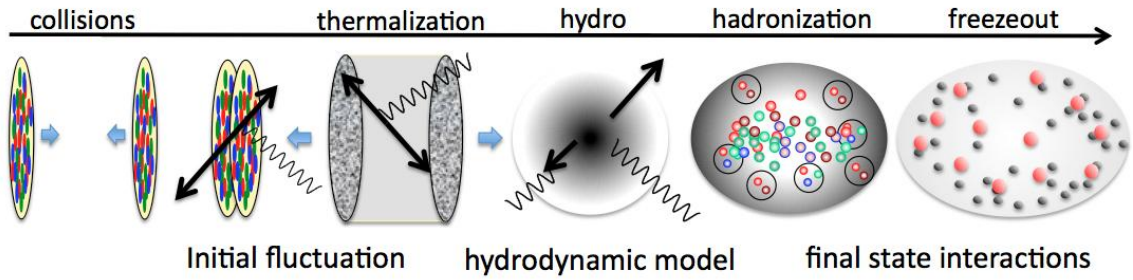

Fig.1.2: Collision picture at high incident energy (E > 2 GeV/nucleon).

Therefore roughly 4% collisions get blocked [7]. Due to this, the dynamics of reaction involved at high energy are governed by nucleon-nucleon collisions. This energy is sufficient to break the internal structure of nucleons and fundamental particles (such as charm, omega (Ω), K-mesons) as shown in the Fig.1.2.

At intermediate energy regime (10 MeV/nucleon $\leq$ E $\leq$ 2 GeV/nucleon), the density of nuclear matter is about 2-3 times the normal nuclear matter density. In intermediate energy heavy ion physics both mean field and nucleon-nucleon interactions play important role. Incident energy in this region is sufficient to break the initial correlation among nucleons but unable to break internal structure of nucleons.

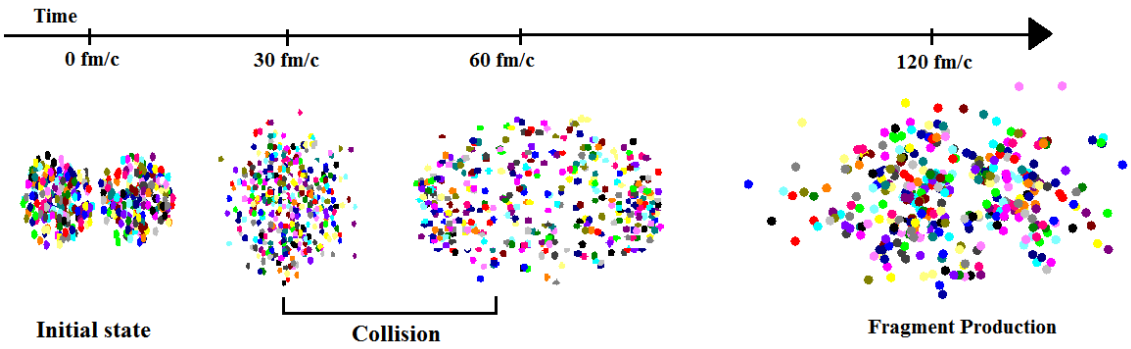

Fig.1.3: Time evolution of two colliding nuclei at intermediate energy.

Here, the main interest is to study the phenomena like multifragmentation, collective flow, nuclear stopping, and production of sub threshold particles, such as pions, kaons, neutrons and protons etc. [8]. The Fig.1.3 shows the time scale of nuclear multifragmentation produced after the collision of two heavy ions at intermediate energies. In Fig.1.3, the two heavy ion nuclei are initialized and then subjected to collision by providing beam energy lying in the intermediate energy domain. During collision, the nucleon (proton or neutron) of one nucleus can interact with the nucleons of other nucleus. After collision, the nucleon forms fragments of different mass.

1.2 Importance of heavy ion collisions at intermediate energies

It is well known that, matter exist in three states; solid, liquid and gas. The state of matter depends upon temperature and pressure. On the same footing, state of nucleus depends upon temperature and density of nucleus. At low incident energy, nucleus show liquid like characteristics and have the density of 0.17 nucleons/fm^3 or 2.7 X 10^{17} kg/m^3.

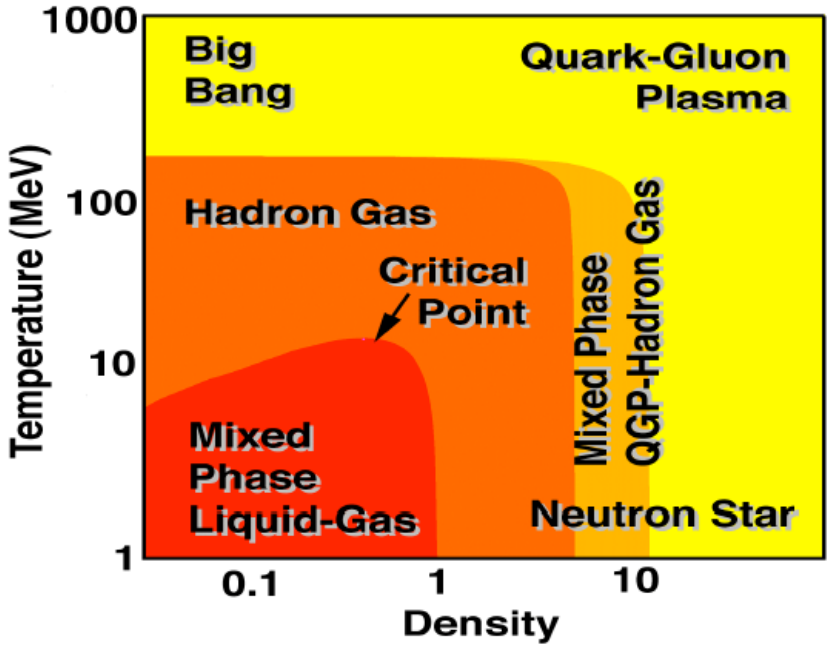

Fig.1.4: The phase diagram for nuclear matter, as predicted theoretically. The horizontal axis shows the matter density, and the vertical axis shows the temperature. Both axes are shown in logarithmic scale, and the density is given in multiples of normal nuclear matter density [9].

The only possible way to heat nuclei to significant temperatures is by colliding them with other nuclei. An average energy of 1 MeV corresponds to a temperature of 1.2×10^{10} K. The temperatures we can reach in nuclear collisions range up to 1000 MeV and above.

As we increase the temperature up to few MeV, some of the nuclear "liquid" evaporates. There are major challenges that nuclear physicists face in their efforts to explore the NEOS and these nuclear phase transitions. One can only establish the hot and dense conditions needed for this process during HIC's.

We also do not have any direct way of measuring the state variables such as temperature, pressure and density. We need to determine them from observables such as:

a) The abundance of isotopes,

b) The population of excited nuclear states,

c) The shapes of the energy spectra from nuclear collision remnants,

d) The production of particles such as pions.

Information about the size of fragments produced when nuclear matter is near its critical point gives essential information on the NEOS. The different phases of nuclear matter like liquid, hadrons gas (HG), quark gluon plasma (QGP) depending upon temperature and density are achieved during the collision.

The liquid phase is represented at T=0 K and $\rho=\rho_o$, on the lower left corner of Fig.1.4, the liquid gas phase (LGP) transition region is characterized by the temperature below ≈ 15 MeV and densities $(\rho/\rho_o) < 1$. HG and QGP is highly dense and hot region.

Fig.1.5 shows the evolution of nuclear matter at different time. It is well known that, the universe started with big bang and has been expanding since. In the earliest instant of time after the big bang, the universe was very hot and predominantly in the form of

radiations. After few micro seconds heavy particles begin to be pair-produced from radiations and matter begins to dominate the energy and continuous till today. This was the path attain by nature. In heavy ion physics, we are following completely opposite path, here we create such a vast conditions around the nuclear matter as in the time of big bang and study the phenomena obtained during the collisions. These observations help us to understand 'what would happen at that time' and this information is also fruitful to know about early universe.

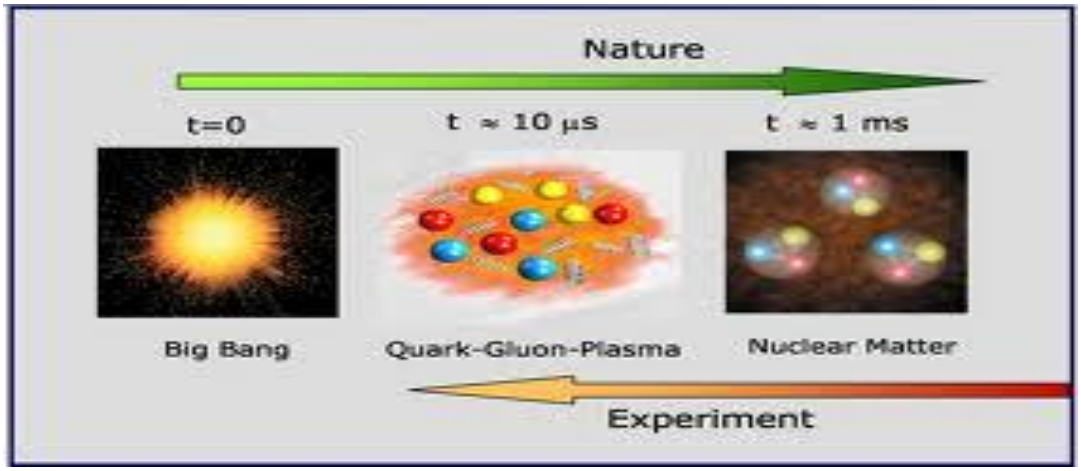

Fig.1.5: Evolution of nuclear matter at different times.

1.3 Collective Flow

The Collective flow is a measure of the transverse motion imparted to particles and fragments during the collision of two nuclei. Any common feature of all the ejectiles emitted in HIC's can be taken as an indicator for the underlying nuclear-matter phase space distribution. A lot of theoretical and experimental efforts have been made in studying the collective flow in heavy ion collisions. The collective flow is a useful tool to explore the nuclear equation of state. Anisotropic flow is defined as the n^{th} harmonic

coefficient v_n of an azimuthal Fourier expansion of the particle invariant distribution [10],

$$\frac{dN}{d\phi} \propto \left[1+2\sum_{n=1}^{\infty} v_n \cos(n\phi)\right]$$

Here, ϕ is the azimuthal angle between the transverse momentum of the particle and the reaction plane. Note that in the coordinate system the z-axis along the beam axis and the impact parameter axis is labelled as x-axis. Anisotropic flows generally depend on both particle transverse momentum and rapidity, and for a given rapidity the anisotropic flows at a transverse momentum $p_t = \sqrt{p_x^2 + p_y^2}$ be evaluated according to the relation: $v_n(p_t) = \langle \cos(n\phi) \rangle$, The first harmonic coefficient $\langle v_1 \rangle$ represents the directed flow, second harmonic coefficient $\langle v_2 \rangle$ represents the elliptical flow which characterizes the eccentricity of the particles distribution in momentum space, third harmonic coefficient $\langle v_3 \rangle$ represents triangular flow and the forth harmonic coefficient represents the quadruple flow $\langle v_4 \rangle$. In the present study we shall mainly concentrated on the elliptical flow.

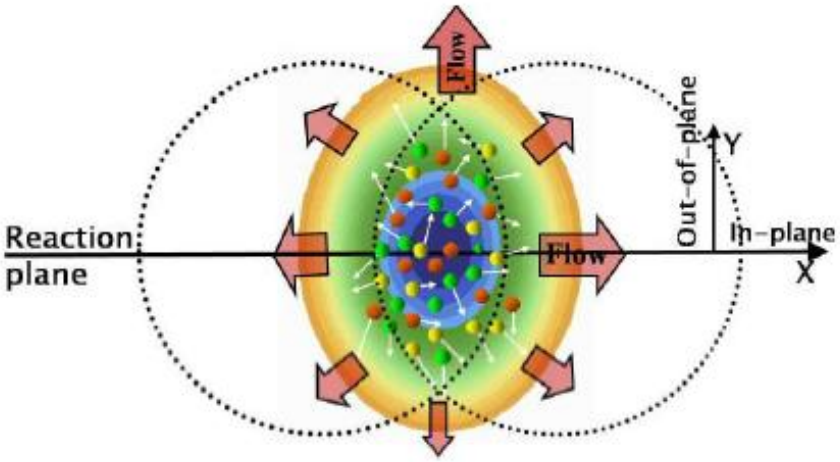

Fig.1.6: The direction of in plane and out of plane emission.

1.4 Elliptical Flow

The elliptical flow describes the azimuthal asymmetric emission pattern in which particles found to be preferentially emitted perpendicular to the reaction plane. Elliptical flow is expected to be larger in peripheral collisions than central collision. The elliptical flow is defined by second order Fourier coefficient from azimuthal distribution of detected particles at mid-rapidity [11] which represents an ellipse that is why it is called elliptical flow.

The two different signatures of elliptical flow as shown in Fig.1.6 are:

- "Bounce-off" of compressed matter in the reaction plane (right).
- "Squeeze-out" of the participants matter out of the reaction plane (left).

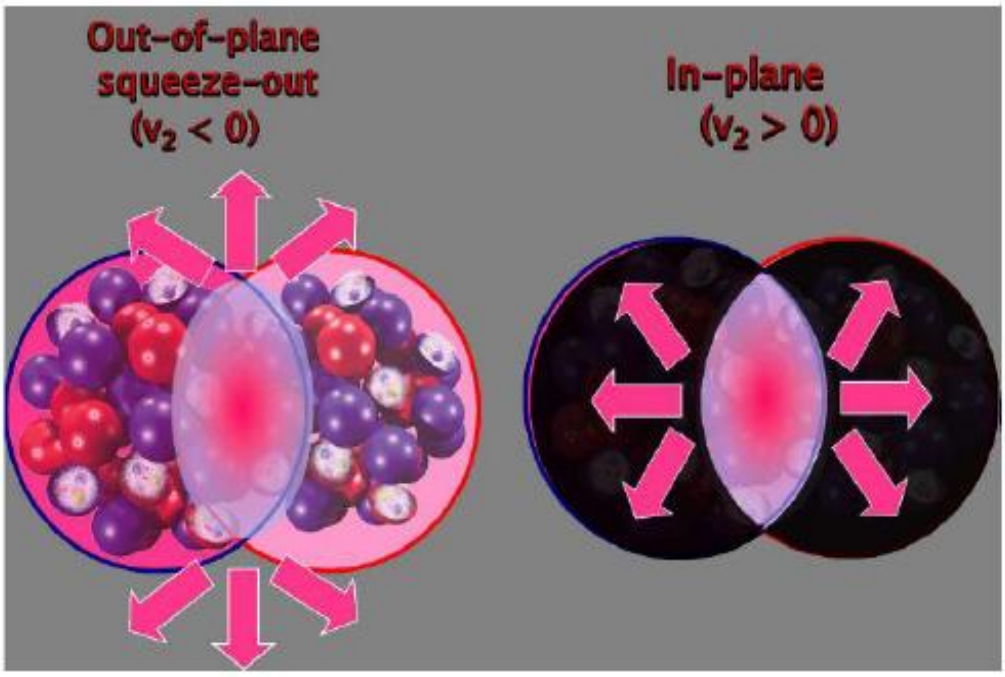

Fig.1.7: Out of plane flow (left) and in-plane elliptical flow (right).

The positive values of the elliptical flow reflect in-plane emission, whereas out-off plane emission is reflected by the negative values. The parameters <Cos 2ϕ > depends on the complex interplay between the expansion, rotation and shadowing of the spectators, apart from the incident energy.

$$\langle v_2 \rangle = \langle \cos(2\phi) \rangle = \left\langle \frac{p_x^2 - p_y^2}{p_t^2} \right\rangle$$

A detailed study on the excitation function of elliptical flow can provide useful information about the nucleon–nucleon interactions and origin of the isospin effects in heavy-ion collisions.

The interesting phenomenon of the elliptical flow is the transition from in-plane to out-of-plane is observed at the mid-rapidity region as shown in fig.1.7, while no transition is observed when integrated over the entire rapidity region. The energy at which this transition is observed is dubbed as the transition energy E_{trans}. It means that participant zone is responsible for the transition from in-plane to out-of-plane. That is why, free nucleons (FNs) $(1 \le A \le 1)$ and light mass fragments (LMF's) $(2 \le A \le 4)$, which are originated from the participant zone, show a systematic behaviour with the beam energy as well as with the composite mass of the system. The elliptical flow for these fragments is found to become more negative with the increase in the composite mass of the system.

1.5 Mass Asymmetry

The HIC's include two types of reactions, symmetric and asymmetric reactions. Symmetric reactions are those in which there is equal number of nucleons in projectile and target nuclei (e.g. ${}^{197}_{79}Au + {}^{197}_{79}Au$). On the other hand, in asymmetric reactions, the number of nucleons in both the nuclei are unequal (e.g. ${}^{197}_{79}Au + {}^{131}_{54}Xe$).The present study mainly concerned to the elliptical flow of the asymmetric nuclei. Many efforts have been made to study the elliptical flow both theoretically as well as experimentally. The

outcome of a reaction depends also on mass of the colliding nuclei, colliding geometry, increase in energy etc. The mass asymmetry parameter can be defined as [12],

$$\eta = \frac{A_T - A_P}{A_T + A_P};$$

Where A_T and A_P are the masses of the target and projectile, respectively. The η = 0 corresponds to the symmetric reactions, whereas non-zero values of η corresponds to asymmetric reactions. The distribution of fragments is symmetric in the reaction plane for symmetric collisions whereas, asymmetric distribution is observed in asymmetric collisions.

As noted by FOPI group, the reaction dynamics in a symmetric reaction ($\eta = 0$) can be quite different compared to an asymmetric reaction ($\eta \neq 0$). This is valid both at low as well as at intermediate energies. This difference emerges due to the different deposition of the excitation energy (in form of compressional and thermal energies) in symmetric and asymmetric reactions. Though the systematic role of mass asymmetry has been explored in multifragmentation [12], yet a lot of work needs to be done to explore the effect of mass as symmetry on the different aspects of elliptical flow.

1.6 Coulomb Potential

As it is well known that the energy associated with the electrostatic interaction between two or more charged particles is called Coulomb potential, it is well defined potential. In nucleus, this energy is due to protons-proton interaction. Coulomb potential is part of binding energy of a system of particles. The Coulomb potential in HIC's at intermediate energies is expected to plays a dominant role in transition energy of elliptical flow due to its repulsive nature. Coulomb potential is more for heavier systems as compared to lighter systems because numbers of protons are more. A marginal difference is obtained on the transverse momentum dependence of elliptical flow summed over entire rapidity in the absence of symmetry energy and presence of Coulomb potential [11]. In present analysis, we study the transverse momentum dependence of elliptical flow at mid-rapidity region, with Coulomb and without Coulomb potential.

1.7 Symmetry Energy

Isospin means pair of similar particles, for example, protons and neutrons are almost identical in the nuclear matter if electric charge difference is ignored. The Isospin dependence of nuclear equation of state is expressed as symmetry energy. The concept of symmetry energy is elaborated in Fig.1.8, the symmetric nuclear matter is represented by the lower line and pure neutron matter is represented by upper line. The difference between these two lines is the symmetry energy, which express the effect of Isospin on the nuclear matter density.

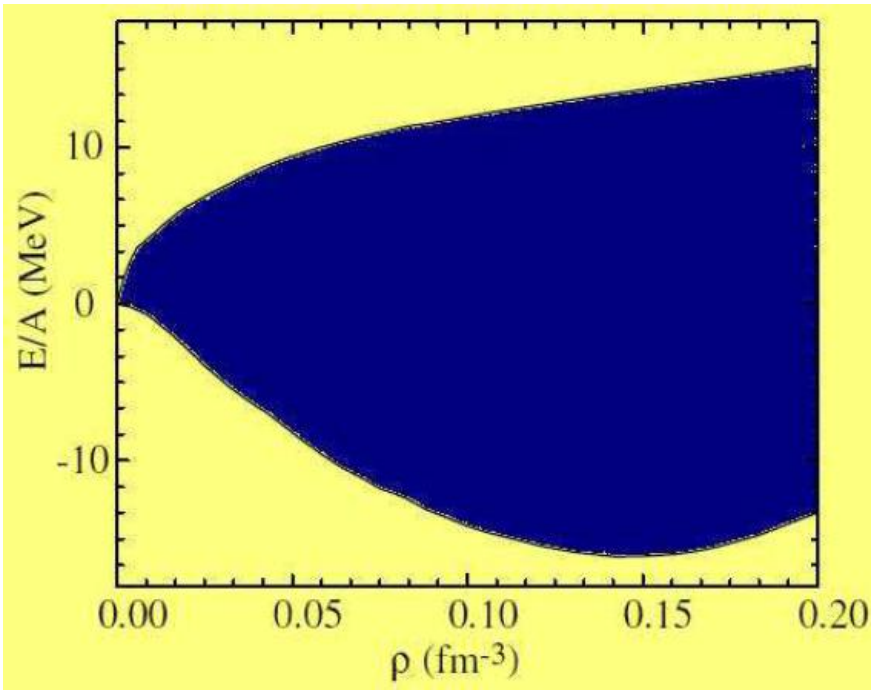

Fig.1.8: The concept of symmetry energy: The top line is the energy density for pure neutron matter and lower line is that for symmetric nuclear matter. The difference of two lines is the symmetry energy [14].

It has been studied that the strength of elliptical flow is very sensitive to symmetry potential. It was observed that elliptical flow per nucleon is larger for EOS without symmetry energy term in comparison to one for EOS with symmetry energy term at

same p_t/A [13]. The isospin effect in elliptical flow at 50 MeV/nucleon for the reaction $^{124}_{50}Sn+^{124}_{50}Sn$ have been predicted for proton and it is found to be very sensitive towards symmetry energy [15]. The effect of symmetry energy on elliptical flow is observed for systems having same mass number but different atomic number, and it has been reported by S. Kumar et al. [11] that neutron rich system shows weaker squeeze-out.

1.8 Review of experimental and theoretical attempts on the elliptical flow

The elliptical flow is very sensitive phenomenon of heavy ion collision in intermediate energy domain. Various theoretical and experimental studies have been done to investigate the dependence of excitation function of elliptical flow on various parameters. The study of elliptical flow on parameters such as beam energy, mass number, impact parameter, nucleon-nucleon cross-section give interesting information about properties and origin of elliptical flow. Many efforts have been made in literature on elliptical flow. Yet to be fully explored in nuclear science community at intermediate as well as high energies.

The elliptical flow term was introduced in 1997 by H. Sorge [16]. Experimentally out off-plane emission, termed as squeeze out was first observed in 1989 by two collaborations at same time. First collaboration was the Diogene collaboration at Saturne Synchrotron in Saclay (France) observed few peaks in the azimuthal distribution of the particles at mid-rapidity in 800 MeV/nucleon Ne-induced reactions [17], and the second was at BEVALAC in Berkeley, the Plastic Ball/Wall group observed out-of-plane emission in $^{197}_{79}Au+^{197}_{79}Au$ collisions at 400 MeV/nucleon [18].

The NSCL at MSU (USA) focussed on the disappearance of elliptical flow for symmetric $^{197}_{79}Au+^{197}_{79}Au$ reactions (at 500 MeV/nucleon to 11 GeV/nucleon). There are many other collaborations like FOPI, ALADIN at GSI, INDRA at GANIL, they concentrated upon the study of transition of elliptical flow from in-plane to out off-plane for different systems [19-21].

The system size, energy, pseudo rapidity and centrality dependence of elliptical flow is studied at 62.4 GeV/nucleon and 200 GeV/nucleon using the PHOBOS detector at the Relativistic Heavy Ion Collider (RHIC) [22]. Under extreme conditions of high temperature and density, nuclear matter is supposed to undergo a phase transition to QGP. To understand this transition, many heavy ion collisions are observed at LBL, SIS, AGS, SPS and RHIC energies. [23].

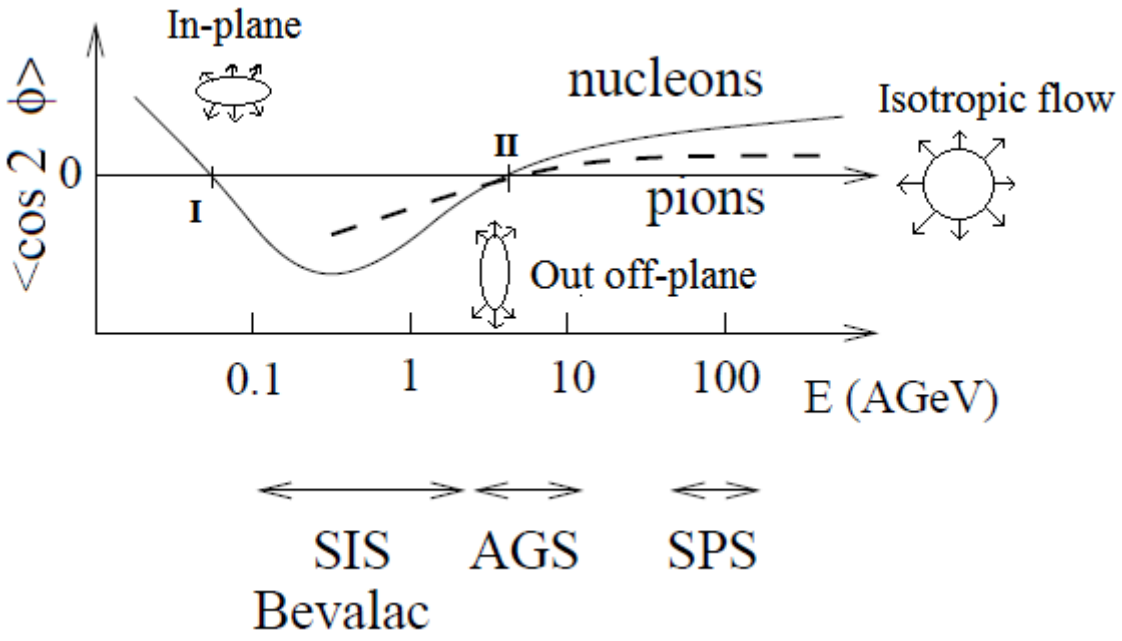

Fig.1.9: Schematic behaviour of the magnitude of elliptical flow as a function of the laboratory frame [24].

Fig.1.9 shows, how elliptical flow varies with incident energy. The solid curve and dotted curve represents the dependence of excitation function of nucleons (proton and neutron) and pions respectively, at different energies. Positive value is for in-plane and negative value is for out off-plane emission. The point where flow line for nucleons and pions meet the axis at zero flow is the point of transition from in-plane to out off-plane emission and corresponding energy is called transition energy. The point marked I in fig.1.9, represents the first order transition in elliptical flow of nucleons and one could

not observe the flow of pions, because there is no production of pions at this incident energy. The point marked II represents the second transition from out off-plane to in-plane elliptical flow of nucleons and first order transition from in-plane to out off-plane elliptical flow of pions. The first order transition corresponds to the change in the direction of preferred fragment emission from the compressed participant region, where as second order transition is due to faster moving spectator as incident energy is very high.

Chapter 2

Methodology

2.1 Introduction

There are several theoretical models which have been developed to study HIC's at intermediate energies. We shall briefly discuss some models with their drawbacks and details of Isospin-dependent Quantum Molecular Dynamical (IQMD) Model in the following sections.

2.2 Time Dependent Harteek-Fork (TDHF) Theory

The time dependent Harteek-fork theory is a quantum mechanical theory which is used to describe the low energy (10 MeV) heavy ion collision [25]. The TDHF is able to explain the fusion, compound nucleus formation, dissipation, shock wave propagation and the fragmentations.

A suitable approach for intermediate energy heavy-ion physics should treat the nucleon-nucleon collision and mean field on equal footing. Some attempts were made in literature to extend the TDHF to take care of residual nucleon-nucleon interactions which are responsible for two body collision. This is called as extended time dependent Harteek-Fork (ETDHF) theory. However, due to complications, this theory could not be used for large scale investigations.

2.3 Boltzmann-Uehling-Uhlembeck (BUU) model

In BUU model, is able to explain one body observables like collective flow, stopping and particle spectra [26]. But N-body features are not described by this model due to lack of fluctuations and correlations. This was the only drawback, that it makes averaging of various results to obtain the appropriate information regarding nuclear matter. Isospin-dependent Boltzmann-Uehling-Uhlembeck (IBUU) model [27] was introduced to study HIC's including isospin effects. The isospin dependence comes into

this model by both the elementary nucleon-nucleon cross-section and the nuclear mean field.

2.4 Intra nuclear cascade (INC) model

It was the first microscopic dynamical model. The intra nuclear cascade model is capable of describing the high energy heavy ion collisions [28]. As the energy is high, so mean field is completely neglected and nucleon-nucleon (NN) collisions are taken without Pauli-blocking [29].

2.5 Vlasov-Uehling-uhlembeck (VUU) model

The microscopic transport model for the one-body Wigner phase space density distribution [30]. Hence the n parallel events are not independent and event-by-event correlation cannot be analyzed within this one-body transport model. VUU uses a phase space sphere around each particle. This model succeeded in the description of one body observables like collective flow, stopping and particle spectra, but the fluctuations and correlations are such that, formation of fragments or the description of two particles correlation in relativistic heavy ion collisions, are beyond the scope of this model. Any fluctuation of the observables seen in the Monte Carlo simulation of one body distribution function is due to numerical noise and disappears in the limit of an infinite number of test particles.

2.6 Quantum molecular dynamical (QMD) model

The N-body features can be described nicely within molecular dynamics model. The Quantum Molecular Dynamics (QMD) model is based on an event by event method [31]. This model needs three steps.

2.6.1 Initialization

Each nucleon is represented by Gaussian wave packet. To initialize a nucleus, we have to assign the coordinates and momenta to all nucleons inside a sphere of radius R = 1.12 $A^{1/3}$fm, where A is the number of the nucleons of nucleus. Moreover, the

coordinates of nucleons are rejected if the distance between any two nucleons is less than 1.5 fm.

2.6.2 Propagation

Successfully initialized nuclei are boosted towards each other with proper centre of mass velocity using relativistic kinematics. The equation of motion of many-body system is calculated by means of a generalized variation principle,

$$\frac{dr_i}{dt} = \frac{\partial \langle H \rangle}{\partial p_i}; \frac{dp_i}{dt} = -\frac{\partial \langle H \rangle}{\partial r_i}$$

2.6.3 Collision

The two nucleons can collide if they come close to each other. The scattering is further subjected to the fulfilment of Pauli-principle. If the final state of scattered nucleons violated the Pauli-principle, the collision is neglected.

QMD neglects the relativistic part and hence it is valid for the incident energies below 1 GeV/nucleon. If one needs to go beyond this energy one needs to take care of proper relativistic tools then we can use Relativistic Quantum Molecular Dynamics model i.e. RQMD [32].

2.7 Isospin quantum molecular dynamics (IQMD) model

This model treats different charge states of nucleons, deltas and pions explicitly [33]. It has been used successfully for the analysis of a large number of observables from low to relativistic energies. The Isospin degree of freedom enters into the calculations via. symmetry potential, cross sections and Coulomb interactions. This model also includes three important steps: First, one has to generate the nuclei. This procedure is called as initialization. Then successfully initialized nuclei propagate under the influence of surrounding mean field. This is termed as propagation. Finally, nucleons are bound to collide if they come beyond a certain distance.

2.7.1 Initialization

In this model, baryons are represented by Gaussian-shaped density distributions,

$$f_i(r,p,t) = \frac{1}{\pi^2\hbar^2} e^{-\left(\vec{r}-\vec{r_i}(t)\right)^2 \frac{1}{2L}} e^{-\left(\vec{p}-\vec{p_i}(t)\right)^2 \frac{2L}{\hbar^2}}$$

Here, Gaussian width L is regarded as the interaction range of the particle. The system dependence of L has been introduced in IQMD in order to obtain maximum stability of the nucleonic density profiles.

Nucleons are initialized in a sphere in accordance with the liquid drop model. Each nucleon occupies a volume of h^3, so that phase space is uniformly filled. The initial momenta are randomly chosen between 0 and Fermi momentum (p_f), without any further local constraints. The Fermi momentum p_f depends on the ground state density. Moreover, the IQMD model performs a Lorentz contraction of the nucleus coordinate distribution, which becomes important at the higher energies.

2.7.2 Propagation

The successfully initialized nuclei are then boosted towards each other with proper centre of mass velocity using relativistic kinematics. The nucleons of target and projectile interact via two and three-body Skyrme forces, a Yukawa potential and momentum dependent interactions. The Isospin degree of freedom is treated explicitly by employing a symmetry potential and explicit Coulomb interactions between protons of colliding target and projectile. This helps in achieving correct distribution of protons and neutrons within nucleus.

The hadrons propagate using Hamilton equations of motion:

$$\frac{dr_i}{dt} = \frac{\partial\langle H\rangle}{\partial p_i};\ \frac{dp_i}{dt} = -\frac{\partial\langle H\rangle}{\partial r_i}$$

$$\langle H\rangle = \langle T\rangle + \langle V\rangle = \sum_i \frac{p_i^2}{2m_i} + \sum_i \sum_{j>i} \int f_i\left(\vec{r},\vec{p},t\right) V^{ij}\left(\vec{r},\vec{r}'\right) \times f_j\left(\vec{r}',\vec{p}',t\right) dr\ dr' dp\ dp'$$

The baryon-baryon potential V^{ij}, in the above relation, reads as:

$$V^{ij}(\vec{r}'-\vec{r}) = V^{ij}_{Skyrme} + V^{ij}_{Yukawa} + V^{ij}_{Coul} + V^{ij}_{MDI}$$

$$= \left[t_1\delta(\vec{r}'-\vec{r}) + t_2\delta(\vec{r}'-\vec{r})\rho^{\gamma-1}\left(\frac{\vec{r}'+\vec{r}}{2}\right)\right] + t_3\frac{\exp(-\left|\vec{r}'-\vec{r}\right|/\mu)}{(-\left|\vec{r}'-\vec{r}\right|/\mu)}$$

$$+ \frac{Z_i Z_j e^2}{\left|\vec{r}'-\vec{r}\right|} + t_4 \ln^2[t_5(\overrightarrow{p'_i}-\vec{p})^2+1]\delta(\vec{r}'-\vec{r})$$

Here Z_i and Z_j denote the charges of i^{th} and j^{th} baryon. Meson potential consists of Coulomb interaction only. The parameters μ and $t_1 \ldots t_6$ are adjusted to the real part of the nucleonic optical potential. Other baryonic potentials like V^{ij}_{Skyrme} and V^{ij}_{MDI} are Isospin independent. Two different equations of states using this phenomenon have been implemented. V^{ij}_{Coul} is the Coulomb potential. The Yukawa potential V^{ij}_{Yukawa} is very short ranged (μ = 0.4 fm in contrast to μ = 1.5 fm in QMD and t_3 = -6.66) and weak. It has been added to improve the surface properties of the interactions which are very important for multi-fragmentation. The two body part $V^{(2)}_{local}$ is directly proportional to $\left(\frac{\rho}{\rho_o}\right)$, whereas, the three body part $V^{(3)}_{local}$ is proportional to $\left(\frac{\rho}{\rho_o}\right)^2$. In nuclear matter, the local potential energy has the form,

$$V_{local} = \frac{\alpha}{2}\left(\frac{\rho}{\rho_o}\right) + \frac{\beta}{\gamma+1}\left(\frac{\rho}{\rho_o}\right)^2$$

The above potential has two free (α and β) parameters, which can be fixed by the requirement that at normal nuclear matter density the average binding energy should be -16 MeV/nucleon and the total energy, should have a minimum at ρ_o.

In order to investigate the influence of different compressibilities, one can generalize the above potential energy to,

$$V_{local} = \frac{\alpha}{2}\left(\frac{\rho}{\rho_o}\right) + \frac{\beta}{\gamma+1}\left(\frac{\rho}{\rho_o}\right)^{\gamma}$$

This equation leads to the nuclear matter equation of state which connects the pressure and energy [31]. By varying there parameters, one can study different NEOS. In the study of heavy-ion collisions one usually uses the so-called Skyrme parameterization of NEOS, which contains two different incompressibilities *k*.

$$k = 9\rho^2 \frac{\partial^2}{\partial \rho^2}\left(\frac{E}{A}\right)$$

One corresponds to soft NEOS with k = 200 MeV (at smaller value of γ), another corresponds to hard NEOS with k = 380 MeV (at larger value of γ). In present work, we have taken k = 200 MeV/nucleons, for soft nuclear equation of state (soft NEOS) and the adjusted parameters are α =-356 MeV, β =303 MeV and γ =1.17.

2.7.3 Collision

Two particles collide if the minimum relative distance $\vec{r}$ of the centroids of the Gaussians during their motion, in their centre of mass frame fulfils the requirement:

$$\left|\vec{r}_i - \vec{r}_j\right| \leq \sqrt{\frac{\sigma_{tot}}{\pi}}\ , \sigma_{tot} = \sigma\left(\sqrt{s}, type\right)$$

Where "type" in above equation denotes the in going collision partners (N-N, N-Δ, N–π etc.). The colliding particles can also scatter elastically or inelastically. The scattering of nucleons in nuclear matter in low density expansion can be described in terms of reaction G-matrix. At high energies the influence of Pauli blocking is less and kinetic energy is large as compared to the potential. Then the imaginary part of the reaction matrix becomes identical to the transition matrix which describes the scattering between two nucleons. Scattering can be elastic or inelastic.

The respective strength of different cross-sections in shown in the Fig.2.1 The total cross-section is the sum of the elastic and all inelastic cross-sections. The elastic and inelastic cross-sections for proton-proton (pp) and proton-neutron (pn) are used in IQMD model. The neutron-neutron (nn) cross-section is assumed to be equal to pp. The total crosssection is equal to sum of elastic and inelastic cross-section is given as,

$$\sigma_{tot} = \sigma_{el} + \sigma_{inel}$$

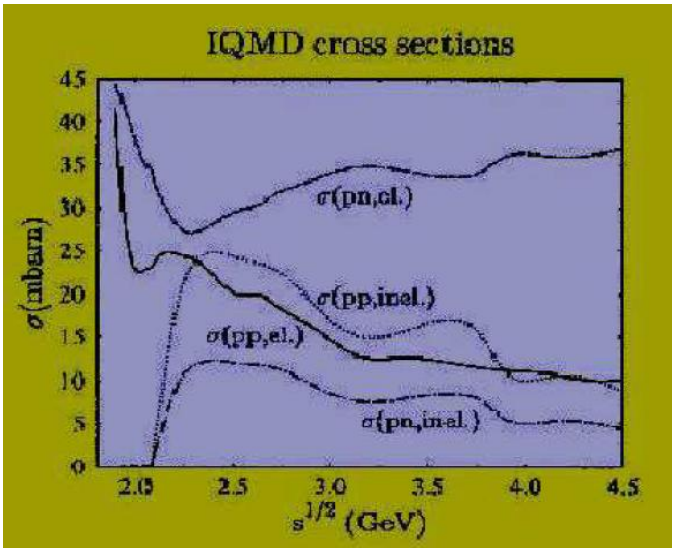

Fig.2.1: The elastic and inelastic cross-sections for proton-proton (pp) and proton-neutron (pn) used in IQMD. The neutron-neutron cross-section is assumed to be equal to pp. The total cross-section is equal to sum of elastic and inelastic cross-section [33].

The nucleons of the target and projectile interact via two and three-body Skyrme forces, Yukawa potential and Coulomb interactions. The Isospin degrees of freedom are treated explicitly by employing a symmetry potential and explicit Coulomb forces between protons of the colliding target and projectile. This helps in achieving the correct distribution of protons and neutrons within the nucleus. In addition to the use of the explicit charge states of all baryons and mesons a symmetry potential between protons and neutrons corresponding to the Bethe-Weizsacker mass formula has been included,

$$V_{sym}^{ij} = t_6 \frac{1}{g_o} T_{3i} T_{3j} \delta(r_i - r_j); \; t_6 = 100 \text{ MeV}$$

Where T_{3i} and T_{3j} are T_3 component (i.e. ½ for protons and -½ for neutrons) denotes the isospin projections of i^{th} and j^{th} baryon respectively. Here V_{sym}^{ij} =32 MeV is used to

consider symmetry energy effect or Isospin-dependent potential and V_{sym}^{ij} =0 for no symmetry energy effect.

2.8 Method of clusterization

The phase space of nucleons of target as well as projectile nuclei are generated by using IQMD model and further this phase space is analysed by using Minimum Spanning Tree (MST) [34] method to clusterize the nucleons. In MST, if the distance between two nucleons is less than certain distance then they are considered to be part of same fragment. Two nucleons share the same fragment if their centroids are closer than d_{min}.

$$\left|\vec{r}_i - \vec{r}_j\right| \leq d_{\min},$$

Where $\vec{r}_i$ and $\vec{r}_j$ are the spatial positions of both nucleons. The minimum distance d_{min} has been used as a free-parameter which varies between 2-4 fm.

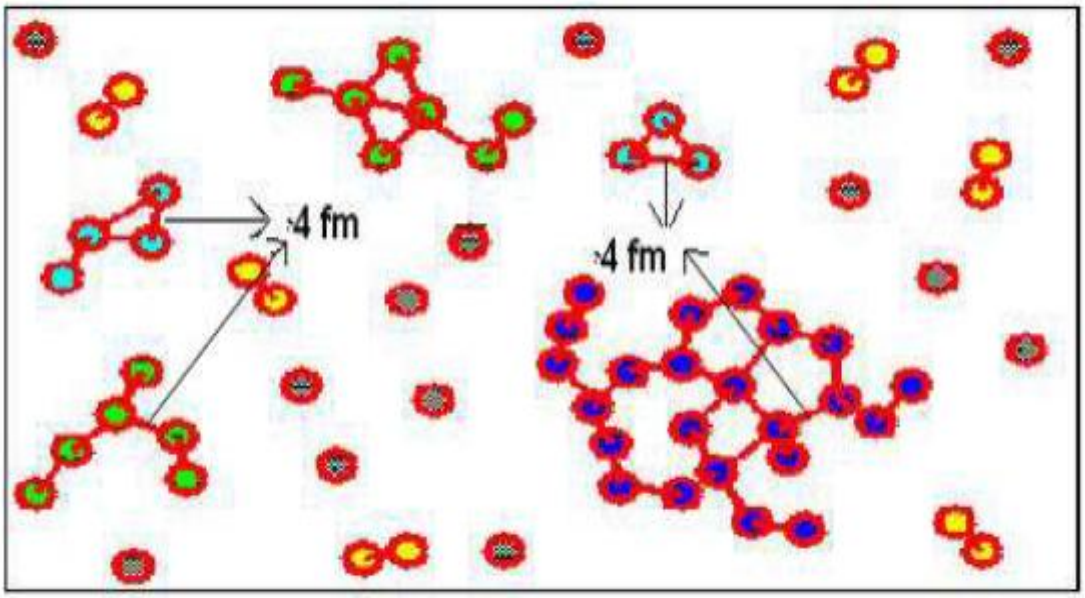

Fig.2.2: This figure is representing the fragments production with MST method where the distance between the nucleons is ≤ d_{min}, here, d_{min} = 4fm.

The fragments production with d_{min} = 4fm is shown in Fig.2.2. However, this method cannot address the question of time scale as it will give a big fragment during the early stage of the reaction where the density is quite high and the interactions between the nucleons are still active. It is worth mentioning that this method can only be used to analyze asymptotic configurations in which the fragmenting system can be viewed as a very dilute mixture of free particles and almost equilibrated fragments. To study the time of fragment formation, one needs to device a method which should be able to detect the overlapping fragments.

Summarizing; we have discussed various theoretical models in brief and details of IQMD model. In the following chapter, we shall present the detailed analysis of role of Coulomb int and symmetry energy in the elliptical flow for symmetric and asymmetric systems. Apart from this, the effect of mass asymmetry on the relative contribution of Coulomb and symmetry energy will be discussed.

Chapter 3

Elliptical Flow in mass asymmetric collisions

3.1 Introduction

In the proceeding chapters, we have studied the importance of HIC's at intermediate energies and also discuss various observables in this energy regime. In the following chapter, we shall focus our study on the elliptical flow, which is one of the burning topics of present day nuclear physics research. The collective flow is closely related to the pressure build up during the compression stage of the colliding nuclei and it is helpful to give us the information about the NEOS. In general the collective flow is of three types, radial flow (which arises in central collisions and refers to isotropic distribution of fragments), directed flow (which measures the collective motion the fragments in reaction plane) and elliptical flow, which is already discussed in section 1.4. The directed flow is reported to diminish at high incident energies, so elliptical flow is well suited to study at higher incident energies [16, 24] and it is helpful in exploring HIC's dynamics.

In the present study, Isospin-dependent Quantum Molecular Dynamic (IQMD) model [33] is used to generate phase space of nucleons of colliding nuclei and clusterization is done using Minimum Spanning Tree (MST) [34] method.

3.2 Radius and Momentum profile

Fig.3.1 represents the radius and momentum profiles of ${}^{197}_{79}Au$, ${}^{175}_{71}Lu$, ${}^{131}_{54}Xe$ and ${}^{40}_{20}Ca$ respectively for 10 differently initialized events. A fewer fluctuations around the mean value are observed in the lighter nucleus as compared to heavier nuclei. From the time evolution of root mean square radius and momentum of nuclei, we come to know about its stability.

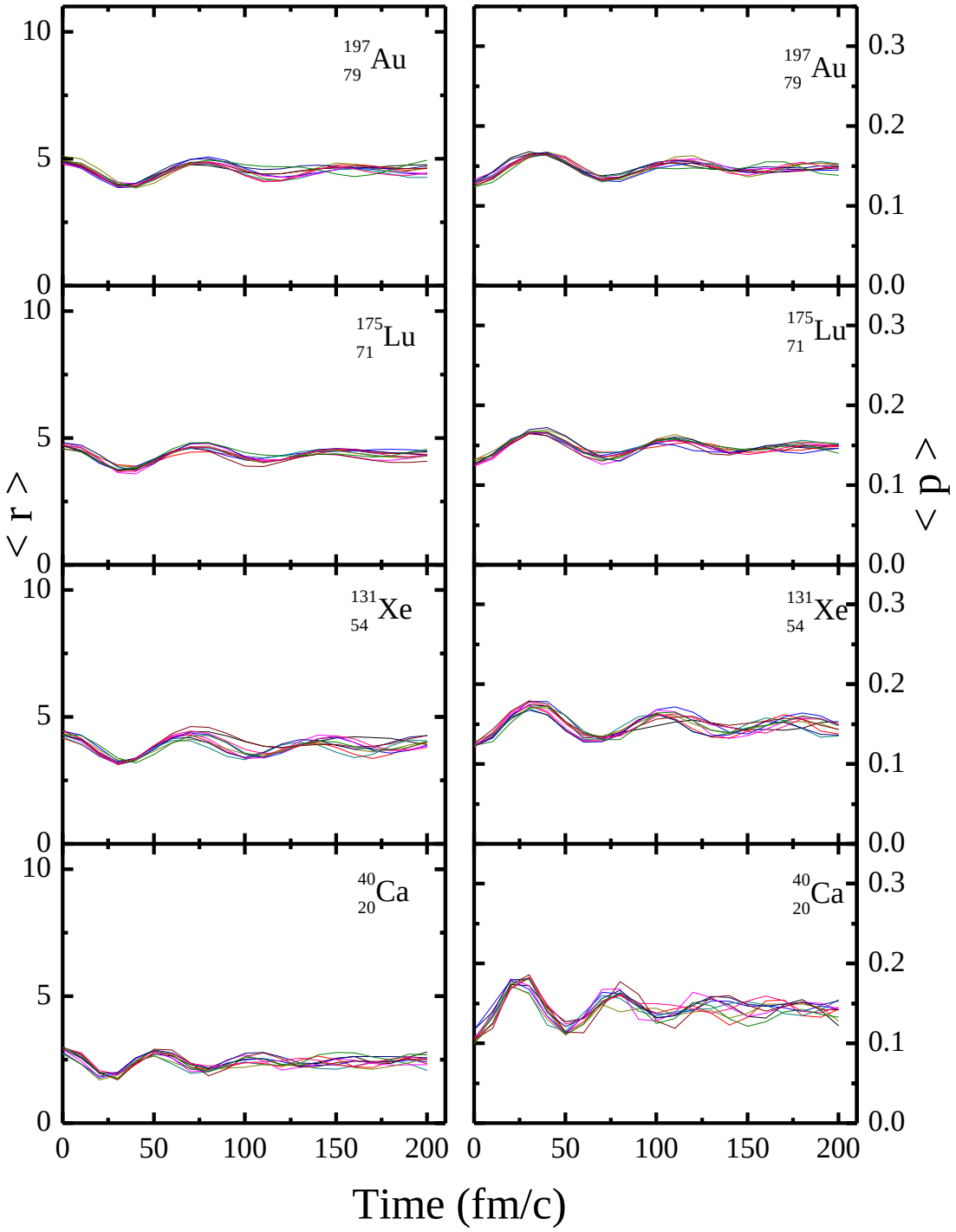

Fig.3.1: Radius profile (left panel) and momentum profiles (right panel) of nuclei $^{197}_{79}Au$, $^{175}_{71}Lu$, $^{131}_{54}Xe$ and $^{40}_{20}Ca$ respectively.

As radius and momentum are plotted with respect to time, an important observation is that, at time t=200fm/c, lines corresponding to all events has become almost straight or parallel to X-axis i.e. radius of all nuclei has become most stable and there is no decaying processes, which is the typical time span of a HIC reaction.

3.3 Snap shot of phase space

Before proceeding further, we observe the evolution of the heavy ion reaction at intermediate energies. Here we have performed the simulation of ${}^{197}_{79}Au+{}^{197}_{79}Au$ by varying energy between 20 MeV/nucleon and 1 GeV/nucleon for scaled impact parameter $\hat{b} = b/b_{\max} = 0.7$ at different time. We simulate the reaction till 200 fm/c, which is considered as saturated time and fragments are constructed using MST method as discussed in previous chapter.

To look at the phase-space of HIC's, we study the phase space in x-y and x-z planes. Fig.3.2 display the evolution of ${}^{197}_{79}Au+{}^{197}_{79}Au$ collision at E=50 MeV/nucleon at scaled impact parameter $\hat{b} = 0.7$ for coordinate and momentum space respectively. In Fig.3.3, x-z plane and x-y plane represents the side view and top view of reaction dynamics respectively. One can observe that there is quite difference in both views. In x-z plane both the nuclei can be seen separately whereas, they appear to overlap on each other in x-y plane.

The role of different energies is displayed in Fig.3.4, where x-z and p_x-p_z of all nucleons are plotted at t = 200fm/c. It can be seen that, a very heavy fragment is produced at 20 MeV/nucleon which disappears at higher incident energies. This figure reveals that at low incident energy a partial fusion occurs whereas, at higher energies either emission of fragments or free nucleons dominate the reaction dynamics. As we increase the energy, the probability of formation of lighter fragments also increases. The p-space at 20 MeV/nucleon is quite compact and at 1 GeV/nucleon, there are two different momentum spaces.

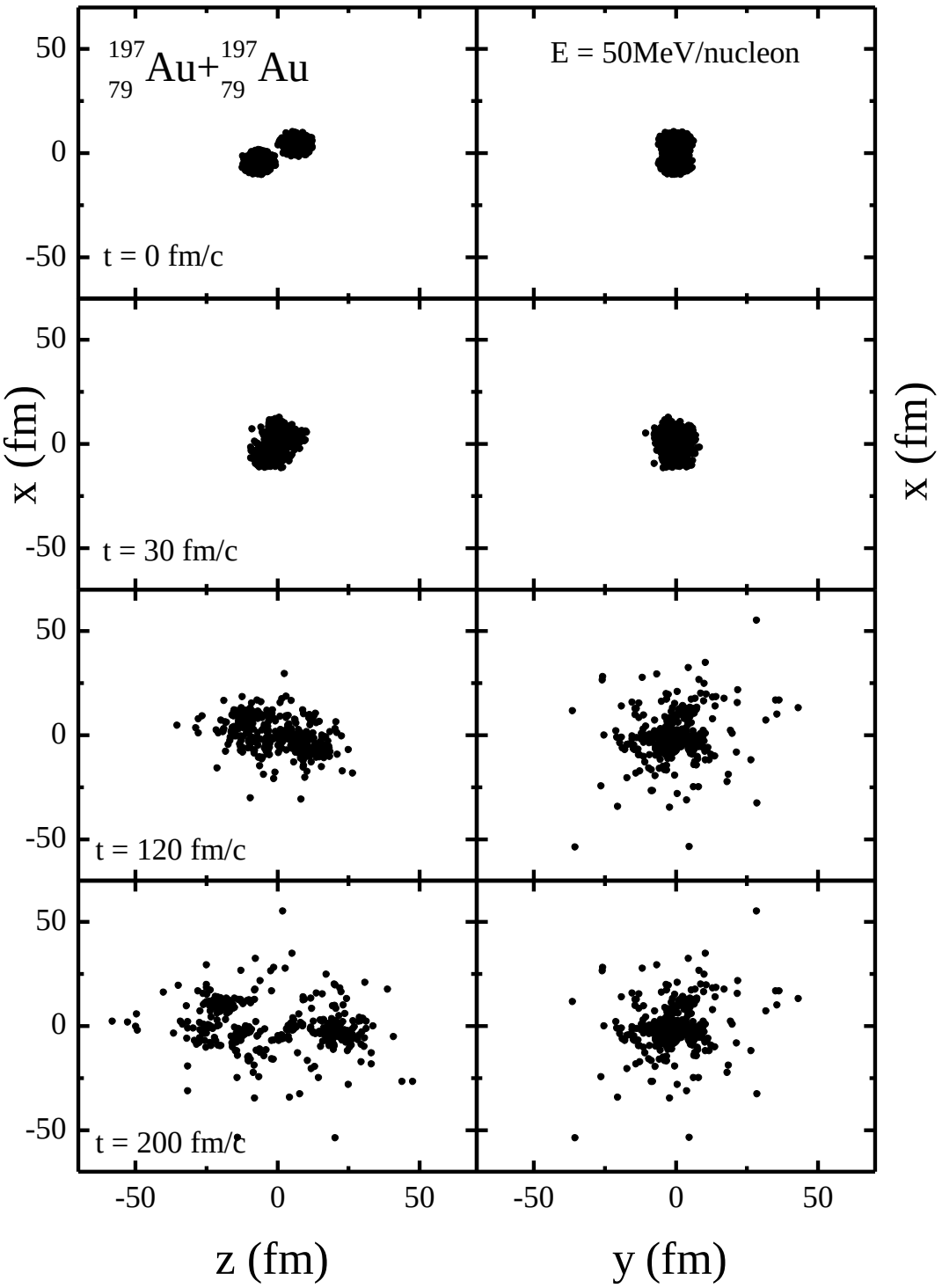

Fig.3.2: The evolution of the $^{197}_{79}Au+^{197}_{79}Au$ reaction at $\hat{b} = 0.7$ for incident energy of 50 MeV/nucleon. These plots are a projection of coordinate space into x-z (left panel) and x-y (right panel) plane.

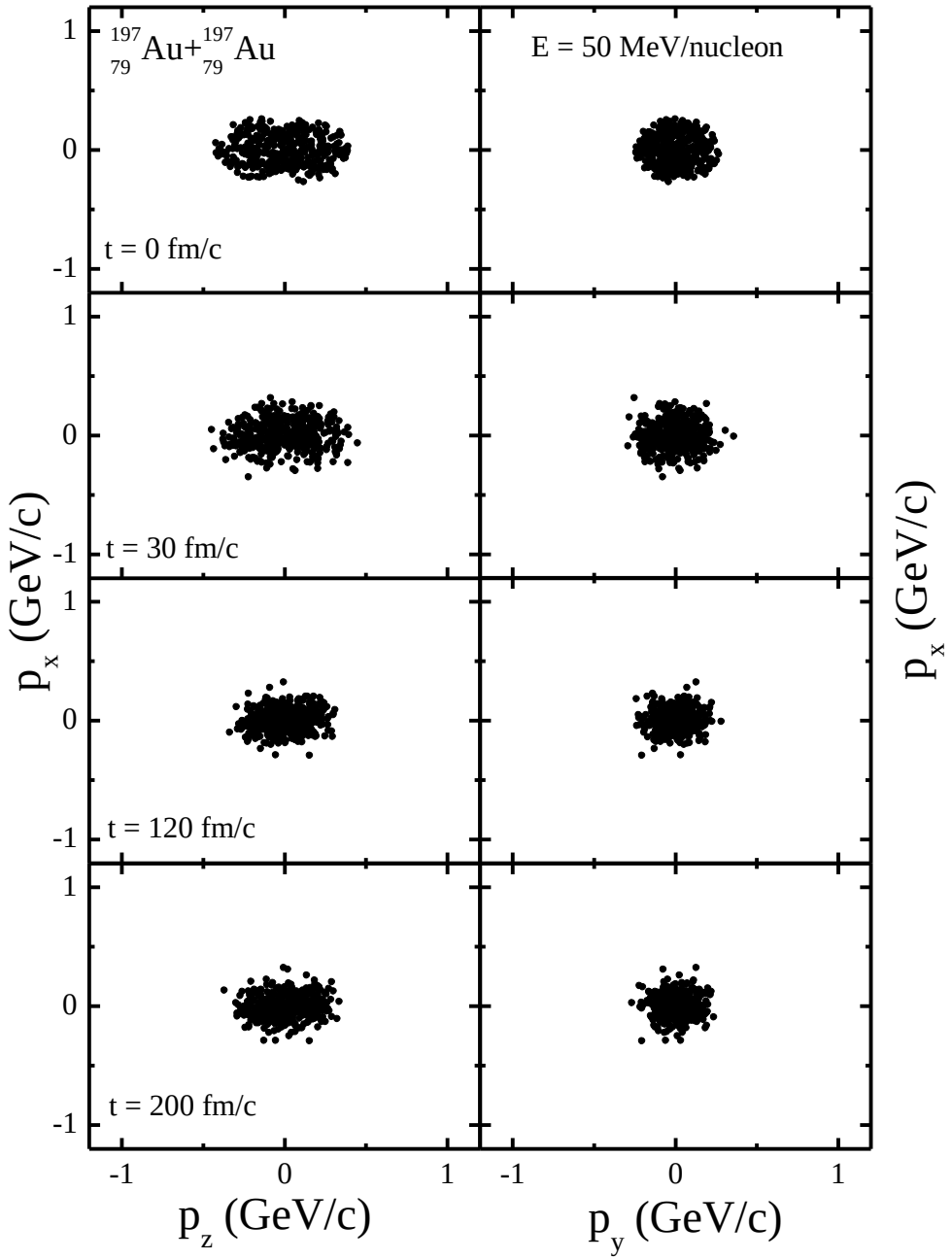

Fig.3.3: The evolution of the $^{197}_{79}Au+^{197}_{79}Au$ reaction at $\hat{b} = 0.7$ and incident energy of 50 MeV/nucleon. These plots are projection of momentum space into p_x-p_z (left panel) and p_x-p_y (right panel) plane.

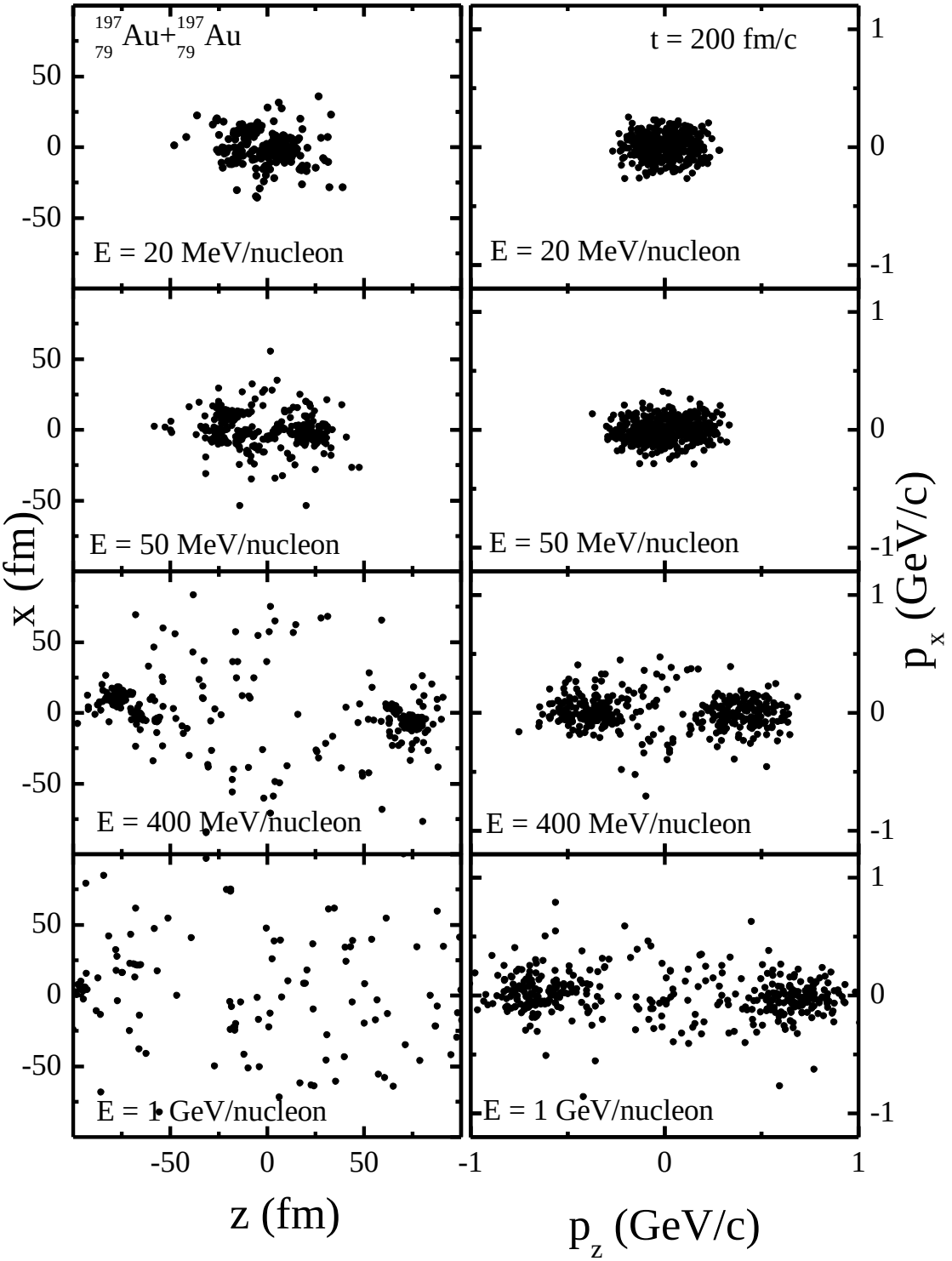

Fig.3.4: The evolution of the phase-space in $^{197}_{79}Au+^{197}_{79}Au$ collisions at incident energy E=20 MeV/nucleon, 50 MeV/nucleon, 400 MeV/nucleon and 1 GeV/nucleon respectively for $\hat{b} = 0.7$. These plots are projection of spatial and momentum space in x-z (left) and p_x-p_z (right) planes.

3.4 Results and discussions:

For the present analysis simulations have been carried out for the reaction of ${}^{197}_{79}Au+{}^{197}_{79}Au$, ${}^{175}_{71}Lu+{}^{197}_{79}Au$, ${}^{131}_{54}Xe+{}^{197}_{79}Au$ and ${}^{40}_{20}Ca+{}^{197}_{79}Au$ i.e. same target with different projectile at incident energy from 50 MeV/nucleon to 400 MeV/nucleon at the scaled impact parameter of $\hat{b}=\frac{b}{b_{\max}}=0.7$, where $b_{\max}=1.12\left(A_T^{1/3}+A_P^{1/3}\right)$fm ($A_T$ and A_P are masses of target and projectile nuclei respectively). The phase-space generated by IQMD has been analyzed using the minimum spanning tree method. All the analysis is done at time t = 200fm/c, which is considered as time when flow saturates and this is true for both heavy and light nuclei.

3.4.1 Transverse momentum dependence of elliptical flow

In this section, we have studied how elliptical flow that depends upon the transverse momentum for FNs$(A=1)$, LMFs $(2\le A\le 4)$ and IMFs$\left(5\le A\le A_{tot}/6\right)$. In Fig.3.5, the final state elliptical flow is displayed for FNs (upper panel), LMFs (middle panel) and IMFs (lower panel) as a function of transverse momentum (p_t) at incident energy E = 50 MeV /nucleon with $\hat{b}=0.7$. The two different coloured curves, black and red corresponds to ${}^{197}_{79}Au+{}^{197}_{79}Au$ (symmetric collisions) and ${}^{40}_{20}Ca+{}^{197}_{79}Au$ (asymmetric collisions) respectively. The mass asymmetry parameter for ${}^{197}_{79}Au+{}^{197}_{79}Au$ is zero $(\eta=0)$ and for ${}^{40}_{20}Ca+{}^{197}_{79}Au$ is 0.66 $(\eta=0.66)$. It is to be noticed that; here elliptical flow is summed over all rapidity bins. A Gaussian shape is observed for $<v_2>$ of all fragments both for symmetric and asymmetric collisions, which is in agreement with one reported by Colona and Di Toro et al. [35]. One can see the effect of fragment size on the elliptical flow. It is observed that elliptical flow becomes more positive as fragment size increases. In asymmetric collisions one can expect large number of big fragments. Therefore curve for LMFs and IMFs is higher in asymmetric collisions as compared to symmetric collisions. The reason behind this observation is that, FNs are unbounded

and have possibility to enjoy in-plane as well as out off-plane but LMFs and IMFs are bounded.

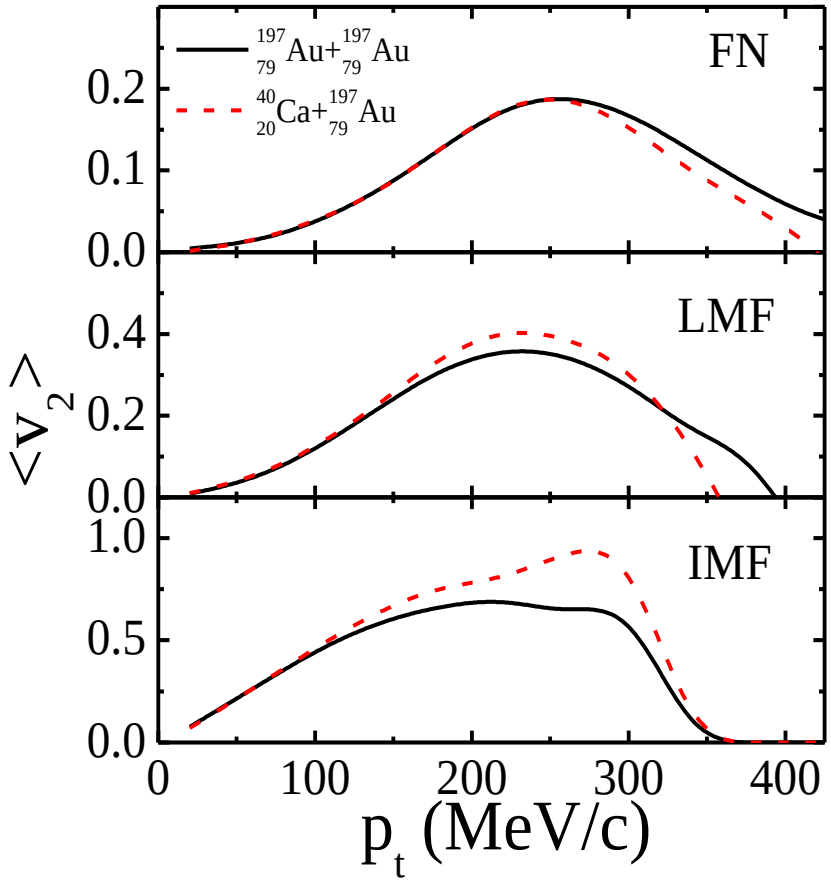

Fig.3.5 Transverse momentum dependence of elliptical flow for FN (upper panel), LMF (middle panel) and IMF (lower panel) with beam energy E = 50 MeV/nucleon and $\hat{b} = 0.7$ for symmetric (black) and asymmetric (red) systems.

From figure one can see that, for FNs, the curves overlap for both symmetric and asymmetric systems at lower momentum, but at higher transverse momentum, there is a difference in both curves which suggest the role of mass asymmetry. On the other hand for LMFs and IMFs, a weaker squeeze out is observed for symmetric system and the prominent peak of distribution diminishes. Even at same impact parameter the extent of

overlap in case of symmetric and asymmetric reactions will not be same. This might be the reason behind the difference in results for both above mentioned reactions.

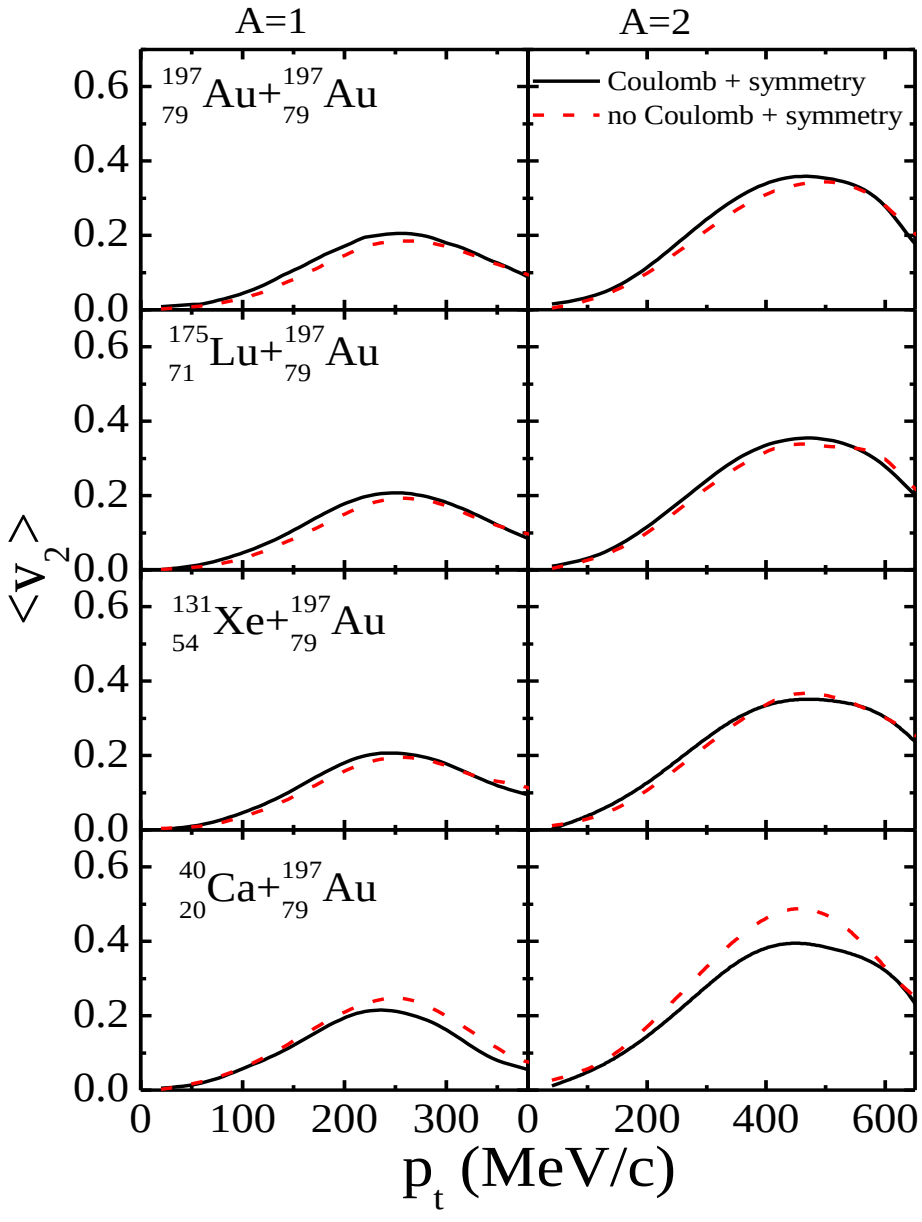

Fig.3.6: The transverse momentum dependence of elliptical flow for FNs (left panel) and LMFs (right panel) at mid rapidity region for incident energy E = 50 MeV/nucleon and $\hat{b} = 0.7$. The panel exhibits the effect of Coulomb potential for symmetric to asymmetric systems.

To strengthen our studies, we have further extended the work to see how transverse momentum dependence of elliptical flow is affected by Coulomb potential and symmetry energy for symmetric and asymmetric collisions. For a meaningful understanding $<v_2>$ is extracted from mid-rapidity region, because mid-rapidity region corresponds to the collision (participant) zone and hence signifies compressed nuclear matter.

Fig.3.6, displays the transverse momentum dependence of elliptical flow with and without Coulomb potential. The left and right panel corresponds to fragments with A=1 and A=2 respectively. Black curve represents the transverse momentum dependence of elliptical flow with Coulomb potential and symmetry energy; whereas red curve corresponds to without Coulomb potential and with symmetry energy. From figure one can see the effect of Coulomb potential for symmetric and asymmetric systems. Weaker squeeze-out is observed in all cases for both A=1 and A=2 except for the system $^{40}_{20}Ca+^{197}_{79}Au$.

The observed effect of Coulomb potential on the prominent peaks of curve for systems $^{197}_{79}Au+^{197}_{79}Au$, $^{175}_{71}Lu+^{197}_{79}Au$, $^{131}_{54}Xe+^{197}_{79}Au$ and $^{40}_{20}Ca+^{197}_{79}Au$ for A=1 is 9.5%, 7.23%, 5.55% and 12.55% respectively. Similarly for the case of A=2 the effect of Coulomb potential on the above mentioned systems is 4.3%, 4.3%, 2.3% and 19.6%. It has been observed that the effect of Coulomb potential decreases with decrease in composite mass (or with increase in mass asymmetry) except for the case of $^{40}_{20}Ca+^{197}_{79}Au$, it shows an extraordinary behaviour.

In Fig.3.7, transverse momentum dependence of elliptical flow for different systems is displayed, similar to that in Fig.3.6, with a difference; here we have observed the effect of symmetry energy rather than of Coulomb potential. It has been observed that a marginal difference is obtained for the case of A=1. The percentage change in Gaussian peak values are less than 2% for all systems. On the other hand, for the case of A=2 this effect is more visible as compared to A=1. For $^{197}_{79}Au+^{197}_{79}Au$ and $^{175}_{71}Lu+^{197}_{79}Au$ the percentage change is 3% and 5% is observed respectively.

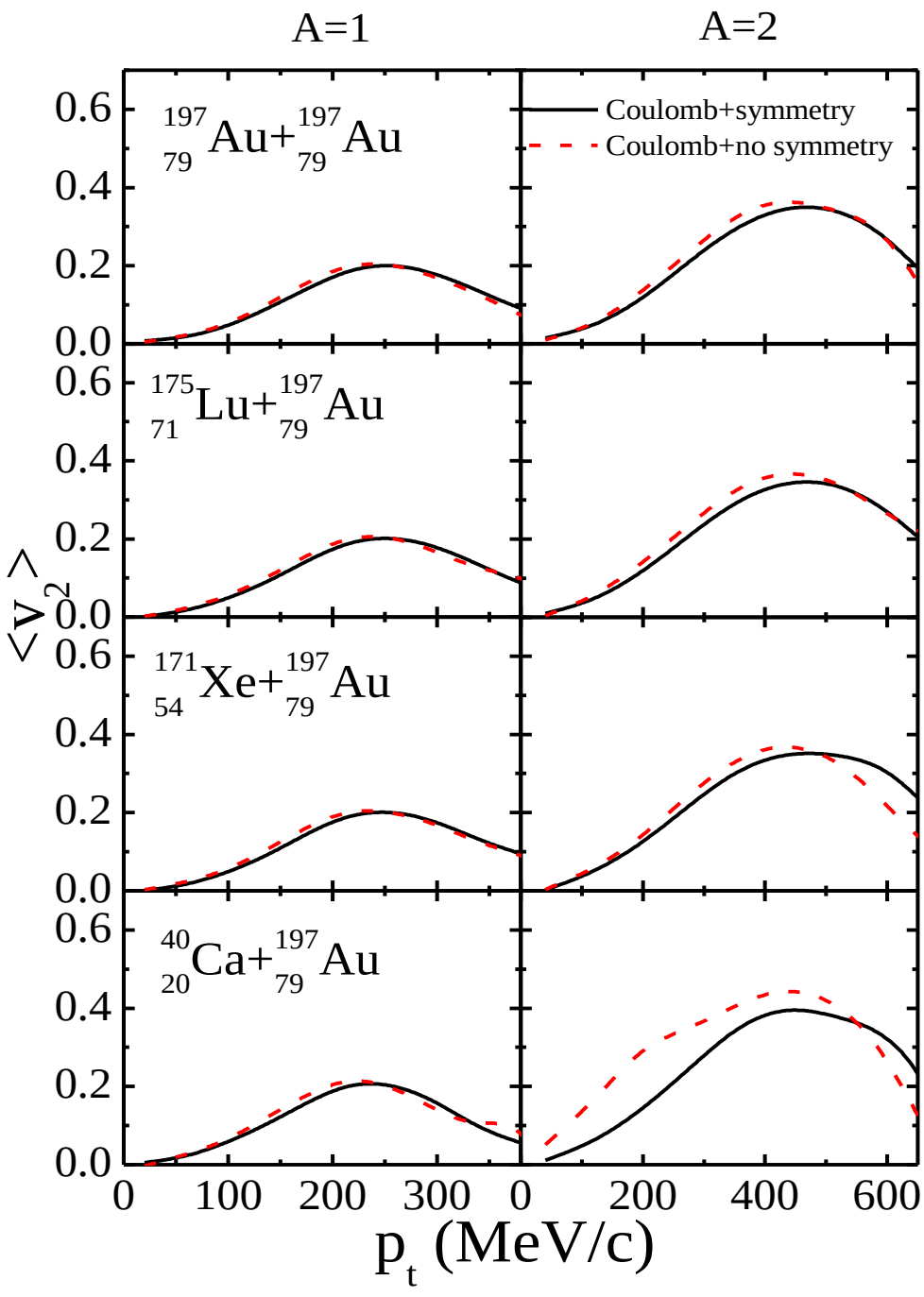

Fig.3.7: The transverse momentum dependence of elliptical flow for A=1 (left) and A=2 (right) in the mid rapidity region with incident energy E = 50 MeV/nucleon and $\hat{b} = 0.7$.

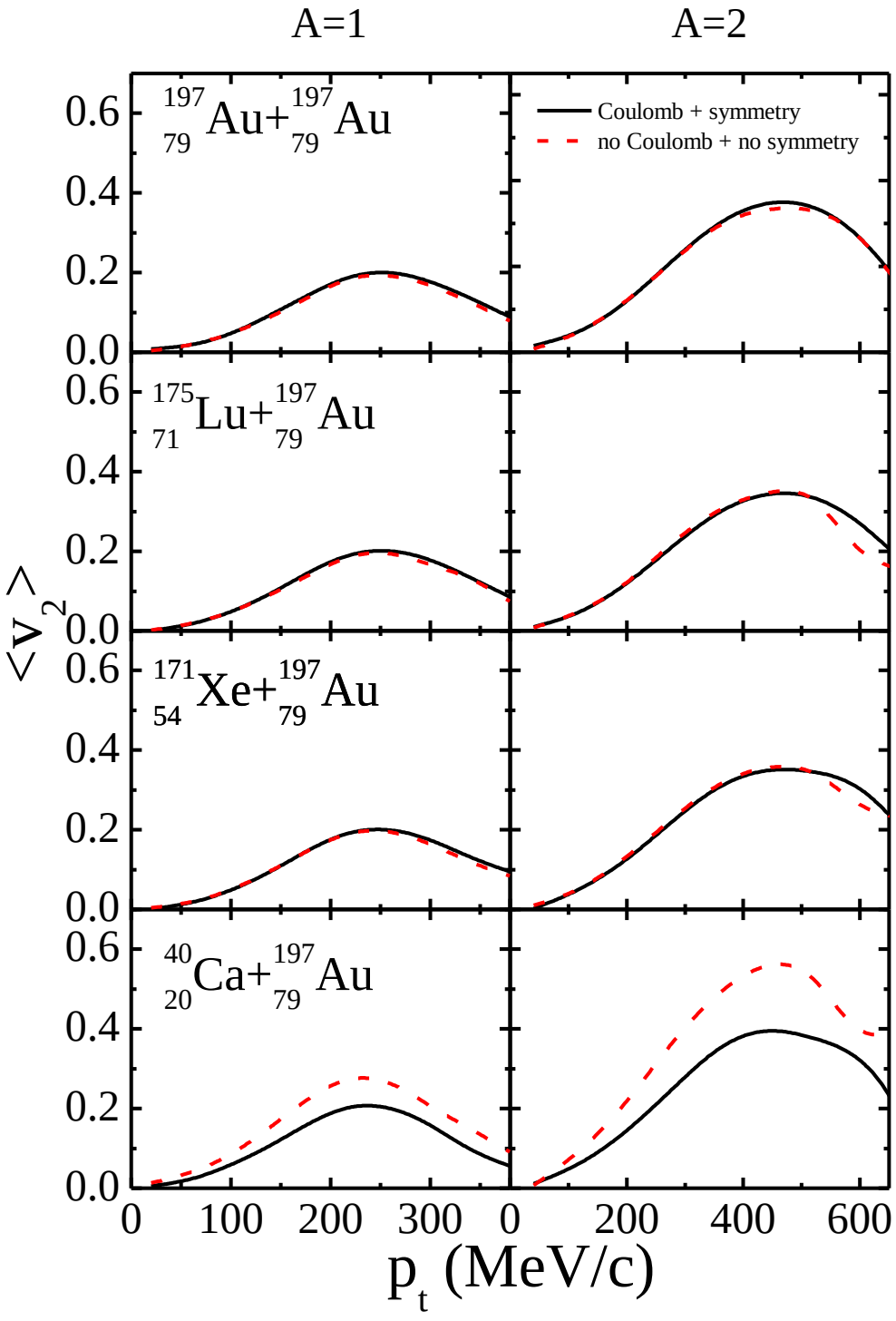

Fig.3.8: The transverse momentum dependence of elliptical flow for A=1 (left panel) and A=2 (right panel) at mid rapidity region with incident energy E = 50 MeV/nucleon and $\hat{b} = 0.7$.

Because $^{197}_{79}Au+^{197}_{79}Au$ $(\eta = 0)$ is symmetric system and $^{175}_{71}Lu+^{197}_{79}Au$ $(\eta = 0.06)$ is nearly symmetric system. While for $^{131}_{54}Xe+^{197}_{79}Au$ $(\eta = 0.2)$, a weaker squeeze-out is observed without symmetry energy and the percentage change on the peaks of distribution is 4% and for the system $^{40}_{20}Ca+^{197}_{79}Au$ $(\eta = 0.66)$ highly asymmetric system, more squeeze-out is observed and the percentage change in distribution peaks is 11%.

The Fig.3.8, black coloured curves correspond to transverse momentum dependence of elliptical flow with both Coulomb and symmetry energy, while red coloured curves correspond to without both Coulomb and symmetry energy. The overall percentage effect on the prominent peaks of distribution curves for A=1 and A=2 is very small. But for $^{40}_{20}Ca+^{197}_{79}Au$, the percentage effect is 25% and 32% for A=1 and A=2 respectively and more squeeze-out is observed as $^{40}_{20}Ca+^{197}_{79}Au$ is highly asymmetric system with $\eta = 0.6$.

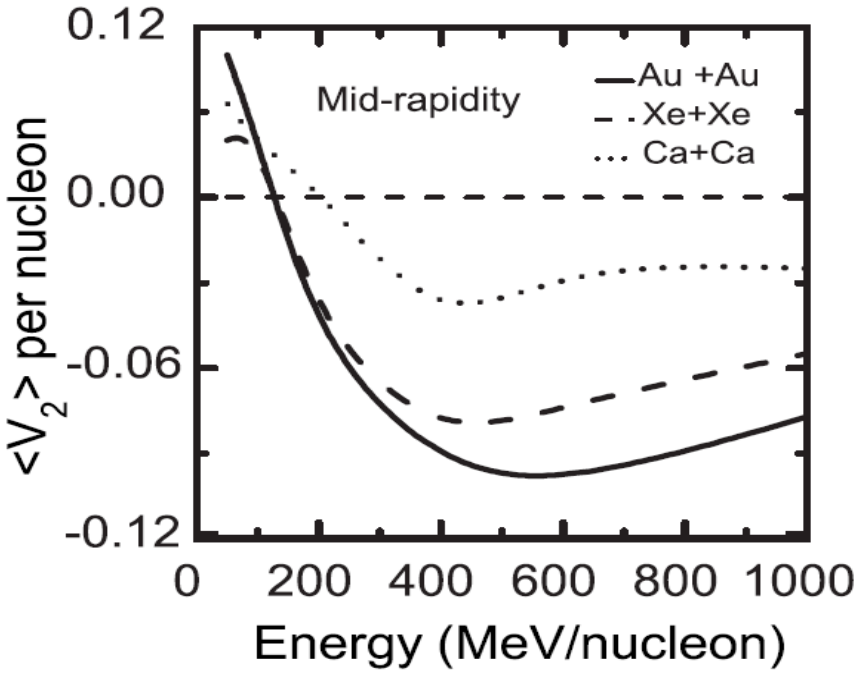

Fig.3.9 Variation of elliptical flow, summed over entire transverse momentum, with incident energy for different symmetric reactions at $\hat{b} = 0.3$ for mid-rapidity region for LMFs $(2 \le A \le 4)$ [11].

3.4.2 Transition energy of elliptical flow

As discussed in section 1.4 and 1.8, the transition from in-plane to out off-plane elliptical flow at intermediate energies is an interesting phenomena and it may be helpful in extracting information about the effective nuclear interactions. The beam energy dependence of elliptical flow for symmetric systems was observed by S. Kumar et al. [11] with $\hat{b} = 0.3$ at mid-rapidity region for LMFs $(2 \le A \le 4)$ as show in Fig.3.9.

The similar kind of study was carried out by V. Kaur et al. [12], for mass asymmetric systems, ${}^{50}_{24}Cr + {}^{102}_{44}Ru\ (\eta = 0.3)$, ${}^{32}_{16}S + {}^{120}_{50}Sn\ (\eta = 0.5)$ and ${}^{16}_{8}O + {}^{136}_{54}Xe\ (\eta = 0.7)$. The incident energy dependence of elliptical flow for LMFs at mid-rapidity region with $\hat{b} = 0.3$ for LMFs $(2 \le A \le 4)$ is shown in Fig.3.10, and transition energy is found to increase with increase in mass asymmetry (η).

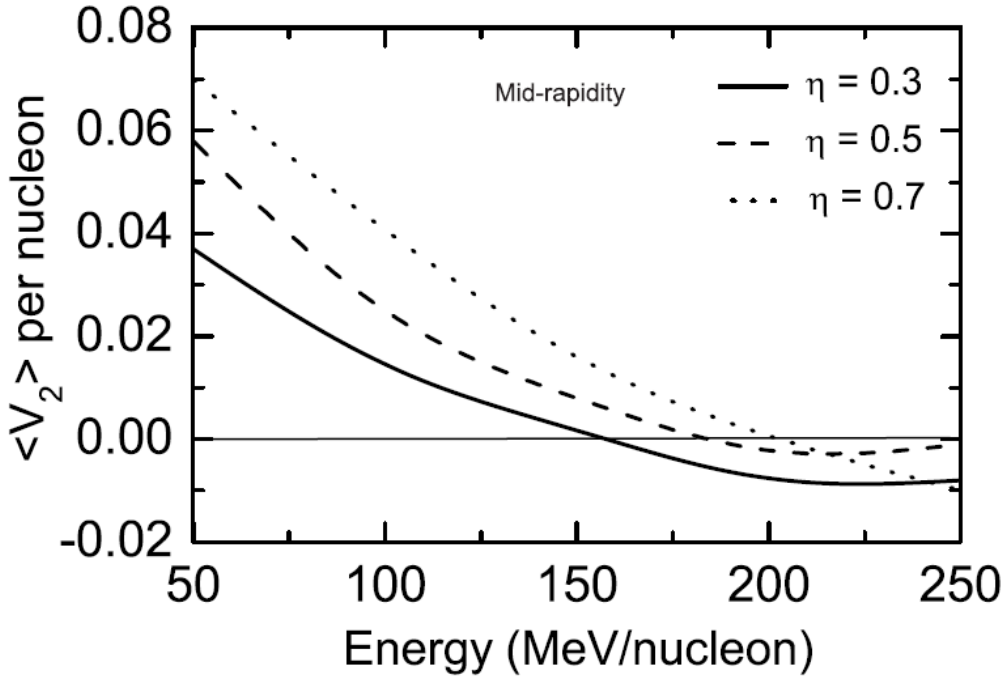

Fig.3.10 Variation of elliptical flow, summed over entire transverse momentum, with incident energy for different symmetric reactions at $\hat{b} = 0.3$ for mid-rapidity region for LMFs $(2 \le A \le 4)$ [12].

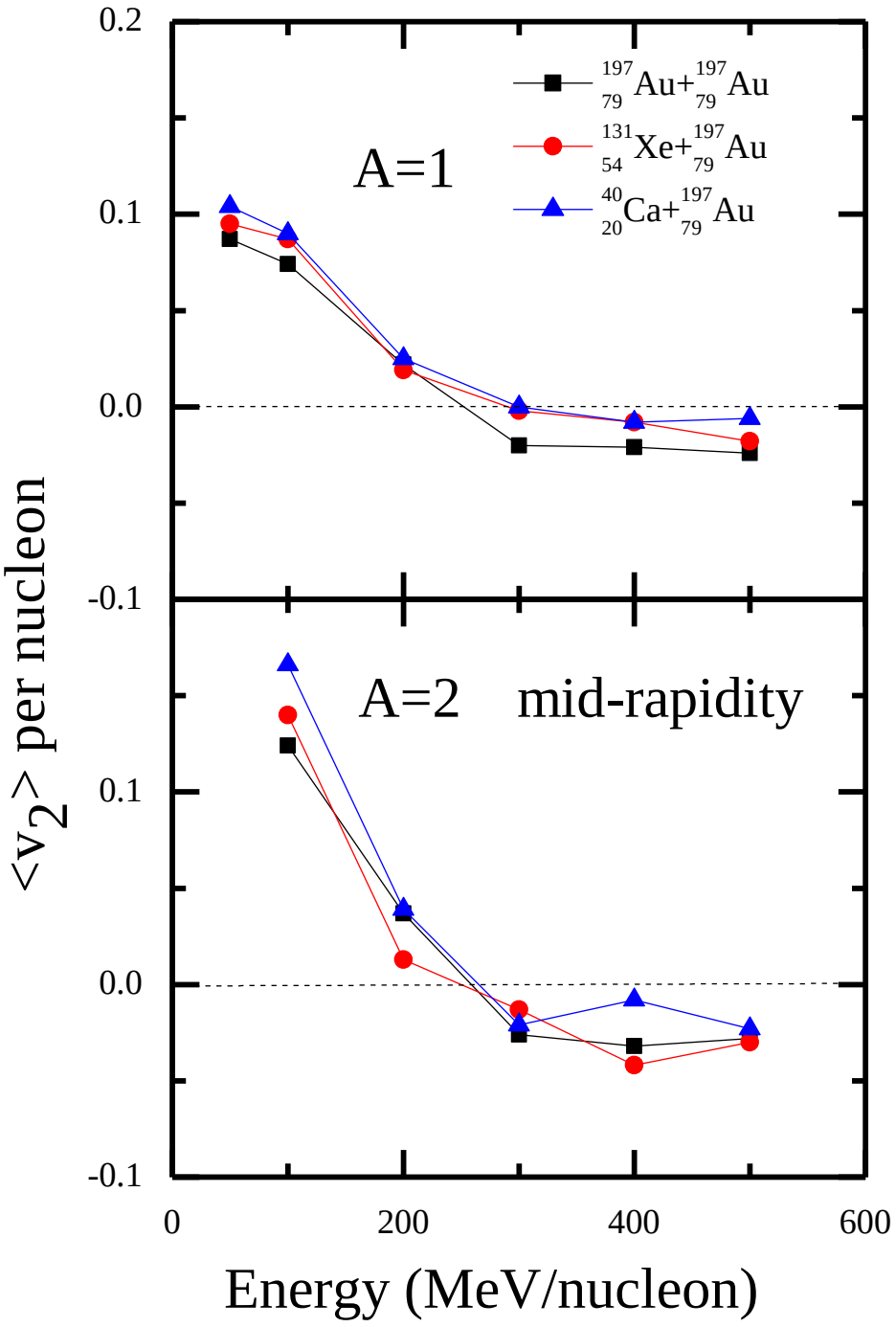

Fig.3.11 Variation of elliptical flow as a function of beam energy for different symmetric reactions at $\hat{b} = 0.7$ for A=1 (upper panel) and A=2 (lower panel).

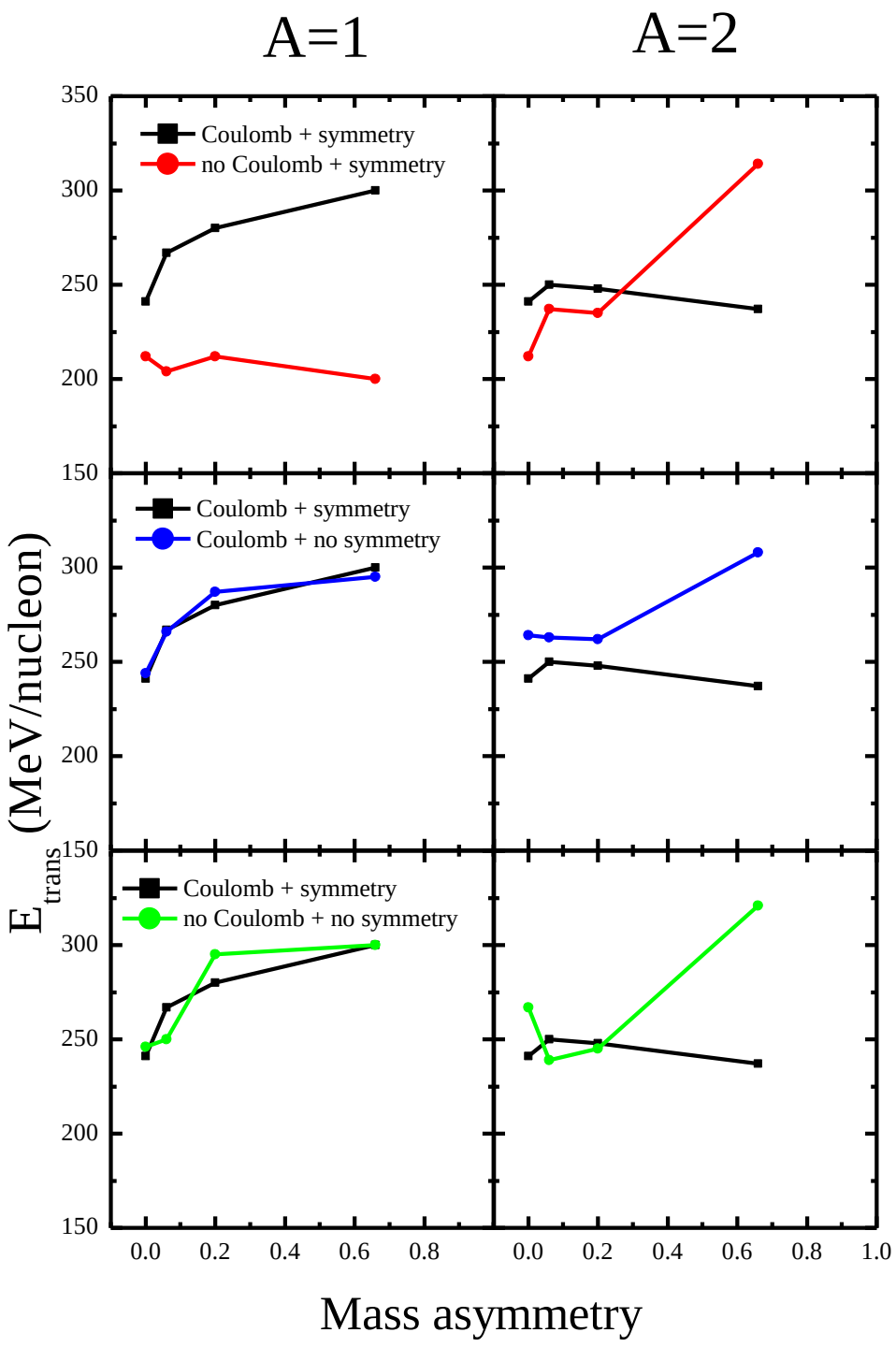

Fig.3.12: The transition energies for elliptical flow at intermediate energies as a function of mass asymmetry (η). The left panel is for A=1 and right panel is for A=2.

Fig.3.11 displays the beam energy dependence of elliptical flow for systems ${}^{197}_{79}Au+{}^{197}_{79}Au\,(\eta=0)$, ${}^{131}_{54}Xe+{}^{197}_{79}Au\,(\eta=0.2)$ and ${}^{40}_{20}Ca+{}^{197}_{79}Au\,(\eta=0.66)$ with scaled impact parameter of $\hat{b}=0.7$ at mid-rapidity region for fragments with A=1 and A=2. A transition from in-plane to out off-plane elliptical flow is observed which is due to change in the direction of preferred fragment emission from the compressed participant region.

We have further extended our studies to see the effect of Coulomb and symmetry energy for symmetric and asymmetric systems. We find out the transition energy for the systems ${}^{197}_{79}Au+{}^{197}_{79}Au$, ${}^{175}_{71}Lu+{}^{197}_{79}Au$, ${}^{131}_{54}Xe+{}^{197}_{79}Au$ and ${}^{40}_{20}Ca+{}^{197}_{79}Au$ by varying beam energy from 50 MeV/nucleon to 600 MeV/nucleon for non-central collision, by taking scaled impact parameter $\hat{b}=\frac{b}{b_{\max}}=0.7$ (a) with Coulomb potential and symmetry energy, (b) without coulomb and with symmetry energy, (c) with Coulomb and without symmetry energy and (d) without Coulomb and symmetry energy for A=1 and A=2.

Fig.3.12 displays the dependence of transition energy on mass asymmetry parameter (η) for A=1 (left panel) and A=2 (right panel). The transition energy of A=1 is increasing with increase in η whereas for A=2 the transition energy decreases with η. The top left panel and top right panel shows the effect of Coulomb potential for A=1 and A=2 respectively. An opposite trend is observed in both cases. Coulomb effect becomes dominating with increase in mass asymmetry of colliding nuclei. The middle left panel and middle right panel displays the effect of symmetry energy and it is found to be very marginal for A=1 but not for A=2. The effect of Coulomb potential and symmetry energy collectively for A=1 and A=2 is displayed in lower left and lower right panel.

3.5 Summary

The dissertation contains a theoretical study of elliptical flow in heavy ion physics at intermediate energies. The IQMD model is used to study the elliptical flow for ${}^{197}_{79}Au+{}^{197}_{79}Au$, ${}^{175}_{71}Lu+{}^{197}_{79}Au$, ${}^{131}_{54}Xe+{}^{197}_{79}Au$ and ${}^{40}_{20}Ca+{}^{197}_{79}Au$ at energy ranging from 50 MeV/nucleon to 600 MeV/nucleon with scaled impact parameter of $\hat{b} = \frac{b}{b_{\max}} = 0.7$. In chapter 3, we have attempted to understand the effect of coulomb potential and symmetry energy for the different systems at energy 50 MeV/nucleon. Coulomb potential dominate the reaction dynamics over symmetry energy. Mass asymmetry plays a significant role in changing the reaction dynamics.

3.6 References

1. Nuclear Physics, 8th edition, D. C. Tayal, Himalaya Publishing House (2011); Nuclear physics by R. R. Roy and B. P. Nigam, published by John Wiley & Sons.
2. R. B. Clare and D. Strottman, Phys. Rep. **141**, 179 (1986).
3. R. Stock. Phys. Rep. **135**, 261(1986).
4. L. C. Vaz, J. M. Alexander and G. R. Satchler, Phys. Rep. **69,** 373 (1981); M. Beckerman, Rep. Prog. Phys. **51**, 1047 (1988). K. E. Zyromski et al., Phys. Rev. C **55**, R562 (1997).
5. C. Ngo, B. Tamain, M. Breiner, R. J. Lombard, D. Mas, and H. H. Deubler, Nucl. Phys**.** A **252**, 237 (1975).
6. H. Ngo and C.h. Ngo, Nucl. Phys. A **348**, 140 (1980); K. C. Panda and T. Patra, J. Phys. G **14**, 1489 (1988).
7. H. stocker and W. Greiner, Phys. Rep. **137**, 277 (1986).
8. S. Kumar, Ph. D. Thesis, P.U. Chandigarh (1999).
9. A Guide to the Nuclear Science Wall Chart @ 2004, Contemporary Physics Education Project (CPEP).
10. S. Voloshin and Y. Zhang, Z. Phys. C **70**, 665 (1996).
11. S. Kumar, S. Kumar and R. K. Puri, Phys. Rev. C **81**, 014611 (2010).
12. V. Kaur, S. Kumar, R. K. Puri, Phys. Lett. B **697**, 512 (2011).
13. B. A. Li, C. M. Ko, and W. Bauer, Int. J. of Mod. Phys. E **7**, 147 (1998).
14. B. A. Li, A. T. Sustich and B. Zhang, Phys. Rev. C **64**, 054604 (2001).
15. Yan Ting-Zhi, Hu Si-Ke, Guo Wen-Xue, Wang Sheng-Long, X U Jin-Ping, Chin. Phys. Lett. **26**, 112501 (2009)
16. H. Sorge, Phys. Rev. Lett. **78**, 2309 (1997).
17. M. Demoulins et al., Phys. Lett. B **241**, 476 (1990).
18. H. H. Gutbroad et al., Phys. Lett. B **216**, 267 (1989).
19. J. Lukasik, G. Auger, and M. L. Begemann-Blaich et al., Phys. Lett. B **608**, 223 (2005).

20. A. Andronic et al., Nucl. Phys. A **679**, 765 (2001); *ibid.* Phys. Lett. B **612**, 173 (2005).
21. J. Lukasik, et.al., INDRA Collaborations, Int. Workshop on multifragmentation and related topics (IWM 2003) Caen, France (2003).
22. B. Alver, B. B. Back et al., Phys. Rev. Lett. **98**, 242302 (2007).
23. P. K. Sahu et al., Pramana-J. Phys. **60**, 1107 (2003)
24. J. Y. Ollitrault, Phys. Rev. D **46**, 229 (1992); J. Y. Ollitrault, Nucl. Phys. A **638**, 195 (1998).
25. A. K. Kerman and S.E. Koonin, Ann. Of Phys. **100,** 332 (1976).
26. A. Uehling and G. E. Uhlenbeck, Phys. Rev **43**, 552 (1933).
27. B. A. Li and S. J. Yennello, Phys. Rev. C 52, R1746 (1995).
28. J. Cugnon, T. Mizutani and J. Vandermeulen, Nucl. Phys. A **352**, 505 (1981).
29. J. Cugnon and C. Volant, Z. Phys. A **334**, 435 (1989).
30. H. Kruse, B. V. Jacak, and H. Stocker. Phys. Rev. Lett. **54**, 289 (1985).
31. J. Aichelin, Phys. Reports **202**, 233 (1991).
32. E. Lehmann, R. K. Puri, A. Faessler, G. Batko and S. W. Huang, Phys. Rev. C **51**, 211 (1995).
33. Ch. Hartnack, R. K. Puri, J. Aichenlin, J. Konapka S.A. Bass, H. Stocker, W. Greiner, Eur. Phys. J. A **1**, 151 (1998); Ch. Hartnack et al., Phys. Rep. **510**, 119 (2012).
34. Y. K. Vermani, R. K. Puri, Eur. Phys. Lett. **85**, 62001(2009).
35. M. Colona, M. Di Toro, G. Ferini, V. Greco, Catania workshop on nucleon and neutrino astrophysics, 15–16 Feb. (2007).